Effects of stress on concrete expansion due to delayed ettringite formation

Yvan Thiebaut, Stéphane Multon, Alain Sellier, Laurie Lacarriere, Laurent Boutillon, Djemal Belili, Lionel Linger, François Cussigh, Sofiane Hadji

Effects of stress on concrete expansion due to delayed ettringite formation

Authors

Yvan Thiebaut [a,b,*], Stéphane Multon [a], Alain Sellier [a], Laurie Lacarrière [a], Laurent Boutillon [b], Djemal Belili [c], Lionel Linger [b], François Cussigh [d], Sofiane Hadji [e]

[a] Université de Toulouse, LMDC (Laboratoire Matériaux et Durabilité des Constructions), UPS/INSA Génie Civil, 135 avenue de Rangueil, 31077 Toulouse Cedex 04, France

[b] Vinci Construction Grands Projets, Direction Scientifique, 5, cours Ferdinand-de-Lesseps 92 851 Rueil-Malmaison Cedex, France

[c] Cofiroute, 12-14 rue Louis Blériot. 92500 Rueil-Malmaison Cedex, France

[d] Vinci Construction France, 61 avenue Jules Quentin 92730 Nanterre, France

[e] Sixence Concrete, 2-4 rue Jean-Baptiste Huet 78350 Jouy-en-Josas, France

Abstract

Delayed ettringite formation (DEF) is a sulfate attack affecting civil engineering structures. This chemical reaction takes place within the concrete matrix of structures and causes damage in concrete and tension in reinforcements. For managers and owners, the ability to predict and reassess the mechanical behaviour of such structures is a major challenge. The influence of both reinforcements and prestress on DEF expansion were studied in the present work. Several tests were performed in laboratory: expansion under both uni and tri-axial restraint due to reinforcements and expansion under prestress (stress level of 14.5 MPa). Uniaxial restraint led to decreased strain in the restrained direction. For prestressed concrete, the loaded direction exhibited creep strain. In both cases, expansions were not impacted in transversal free directions. Therefore, DEF expansion under uniaxial stress is anisotropic. Cracks were observed parallel to the restrained direction. The final volumetric expansion was lower than in stress-free conditions (decrease of 27% for uni-axially restrained condition). For triaxially restrained tests and prestressed specimens, the volumetric decreases were 56% and 34% respectively. Data provided by these results will be used for numerical reassessment of DEF damaged structures.

Keywords

Anisotropy, Delayed Ettringite Formation (DEF), Expansion, Sulfate attack, Modelling.

Highlights

- DEF expansion in reinforced and prestressed concrete specimens has been studied
- Expansions decrease in restrained directions but remain unchanged in free direction

* Corresponding author at: LMDC, Université de Toulouse, INSA/UPS Génie Civil,
135 Avenue de Rangueil, 31077 Toulouse cedex 04, France.
E-mail address: yvan.thiebaut@vinci-construction.fr (Y. Thiebaut).

- The final volumetric expansion is reduced when restraint is applied
- Expansion due to sulfate attack under uniaxial loading is anisotropic
- Expansion appears to be independent of loading applied in other directions

1. Introduction

Sulfate attacks are the result of chemical reactions between sulfates, water and hydration products of Portland cement [1–6]. These pathologies lead to ettringite formation and result in concrete expansion and damage [7–11]. Reinforcements and applied stresses delay or prevent concrete cracking, with a major effect on resulting expansions [8,10,12–14]. Delayed ettringite formation (DEF) is a sulfate attack occurring in structures under certain circumstances that is likely to affect their durability [10,15–17]. In this case, sulfates come exclusively from an internal source, which is primary ettringite dissolution [18–23]. This is mainly due to heat treatment or natural exothermic reactions of cement hydration and occurs when the temperature exceeds a given threshold, typically 65 °C for Portland cement [18,24,25].

The aim of this article is to highlight the influence of reinforcements and stresses on concrete affected by DEF and, more broadly, by sulfate attacks. Some authors have designed experimental plans to quantify these effects on cement based materials. The effects of homogeneous restraint imposed by external reinforcements on immersed mortar have been studied on prisms (40×40×160 mm) affected by DEF [8] and on thin-walled hollow cylinders (diameter 30.0 mm, wall thickness 2.5 mm) affected by external sulfate attack [26]. Other studies have considered reinforced concrete beams (610×914×5486 mm and 250×500×3000 mm) in heterogeneous hydric and mechanical conditions [10,14,27]. In all these studies, expansions decreased in restrained directions. Bouzabata et al.'s and Müllauer et al.'s studies were performed using mortar mix and cannot be generalised to concrete. Moreover, only uniaxial restraint was investigated. On the opposite, Karthik et al.'s, Deschenes et al.'s and Martin's results are largely impacted by both thermal, hydric and mechanical gradients. The direct assessment of a DEF affected concrete behaviour law depending only on stresses is consequently difficult. In this context, the main aim of the experimental plan reported in this article was to extend Bouzabata et al.'s results to concrete. To do so, plain, uniaxially or triaxially reinforced and prestressed concrete specimens in homogeneous thermal, mechanical and saturation conditions has been studied. For this purpose, "pathologic" concrete prisms (100×100×500 mm) were exposed to a heat treatment representative of what could be experienced on site for massive structures and then immersed in water in order to trigger delayed ettringite formation reactions and to allow alkali leaching [28–31]. Because

of alkali leaching, the chemical conditions were not homogeneous and this had an impact on the delayed ettringite formation and thus on the expansion of specimens [32]. The alkali concentration in the storage water was measured throughout the tests so that chemical boundary conditions were known all times during the monitoring. In the case of reinforced specimens, steel bars and stirrups were embedded in the concrete. Homogeneity of the mechanical loading was ensured in the longitudinal direction by the positioning of steel plates and restraint systems on both sides of the specimens and, in transversal directions, by the placing of stirrups, when needed, along the specimens. Prestressed specimens were loaded by means of a creep test device that maintained a constant pressure in the hydraulic system. A calibrated extensometer measured the longitudinal and transversal expansions between stainless steel studs glued on the central part of concrete surface. The first part of the paper presents the experimental conditions. The expansions measured on each specimen and the evolution of the cracking pattern are then detailed in section **3**. Finally, the results are analysed and compared with those found in the literature.

2. Experimental conditions

2.1 Materials

Experiments on the effect of reinforcement and stress on expansion due to DEF were performed on concrete with a water/cement ratio of 0.48 and a cement content of 410 kg/m^3 (**Table 1).**

Table 1. Concrete composition.

Component	Proportion (kg/m^3)
Cement	410
Water	197
Siliceous sand 0/0.315	93.5
Siliceous sand 0.315/1	174
Siliceous sand 1/2	184
Siliceous sand 2/4	196
Siliceous gravel 4/8	188
Siliceous gravel 8/12.5	878
NaOH addition	5.0

The water amount takes into account water absorption of the aggregates. Aggregates were siliceous and qualified as non-reactive regarding Alkali-Silica Reaction [33]. They were supplied from Palvadeau quarry typically used as reference aggregates for numerous research programs. The binder was a standard Ordinary Portland Cement (OPC, CEM I 52.5 R). **Table 2** presents the cement compositions obtained by inductively coupled plasma optical emission spectrometry (ICP-OES) and chromatography analysis. Sodium hydroxide, NaOH, was added to the mixing water at a dose of 5.0 kg/m^3 of concrete. Specimens were cylinders for the mechanical property measurements and prisms for assessing the impact of the reinforcement and stress on expansion. They were all cast at the same time.

Table 2. Cement chemical composition (%).

	SiO_2	**Al_2O_3**	**Fe_2O_3**	**CaO**	**MgO**	**SO_3**	**K_2O**	**Na_2O***	**Na_2O_{eq}***
ICP-OES and chromatography analysis	20.1	4.52	2.37	64.6	0.78	3.19	0.16	0.15	0.25

** before NaOH addition*

2.2 Curing and storage conditions

Approximately 80 minutes after casting, most of the specimens were cured at high temperature: increase from 20 to 80 °C in 33 hours, a slow decrease from 80 to 72 °C in 63 hours, and a return from 72 °C to 20 °C in 240 hours. This heat treatment corresponded to the temperatures recorded at the heart of massive concrete structures (14.0×3.5×2.0 m) during hydration [34]. All "DEF reactive" specimens were placed together in a climatic chamber. This heat treatment was realised in autogenous conditions: the concrete specimens were sealed during the cure by placing a silicone seal and a screwed wooden top on the moulds and the relative humidity in the climatic chamber was maintained close to 95% all along the thermal cycle. Temperature measurements in the centre of the samples had been made on a previous study using the same concrete composition (from another batch) and thermal and hydric conditions: differences between instructions and measurements never exceeded 2°C. At the same time, other specimens from the same batch were stored at 20 °C in similar autogenous conditions. After the 14 days required for the heat treatment, all the specimens were unmoulded and stored for an additional 14 days period at a temperature close to 20 °C and 50% of relative humidity. Drying shrinkage might have induced micro cracking during this period. Porosity might have been impacted, with consequences on the specimen's behaviour. First of all, initial water absorption expansion after

immersion could have been increased compared to undried concrete. Secondly, alkali leaching during the tests could have been accelerated because of a better water diffusion in concrete. As ettringite stability is improved when alkali content decreases, this phenomenon could lead to faster DEF reaction. Finally, large initial voids might have been created in the concrete matrix by drying shrinkage macro cracking, providing precipitation sites for delayed ettringite. According to Brunetaud, DEF expansion are mainly due to ettringite formation in small pores. In this case, both strain kinetic and final amplitude might have been impacted. Specimens were then immersed in agitated, non-renewed water maintained at 38 °C from 28 days after casting. The water volume remained constant and was close to 0.28 m^3. The concrete/water volume ratio of the storage bath was 0.23. **Figure 1** summarizes the evolution of the curing, storage and mechanical conditions (in the case of prestressed specimens) after casting. Both heated and non-heated specimens were stored together in the bath of water, with a heated/total concrete volume ratio equal to 0.77.

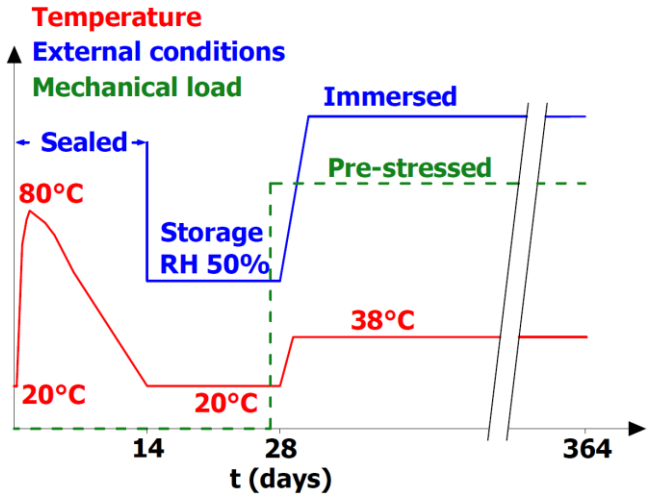

Figure 1. Thermo-hydro-mechanical history of concrete specimens.

Alkali content in the storage bath was regularly measured on water samples by ICP-OES. The results highlighted alkali leaching from the concrete into the water (**Figure 2**). This phenomenon implied a decrease of alkali content in the concrete paste, which may lead to an acceleration of the delayed ettringite formation [28–31]. The estimated free-alkali content in the pore solution fell from 1.05 mol/L to 0.56 mol/L between 0 and 323 days after immersion. These values were assessed taking the cement alkali content and sodium hydroxide addition into account. The porosity was assumed to be close to 15% of the volume. Thermal damages and hydration changes induced by heat treatment could have induced modifications in concrete microstructure. The possible differences between alkali leaching for heated and non-heated concrete induced by these phenomena could not be deduced from measurements of alkali content in the storage bath. To do so, direct measurements of alkali content remaining in both kind of specimens at the end of the monitoring will be done.

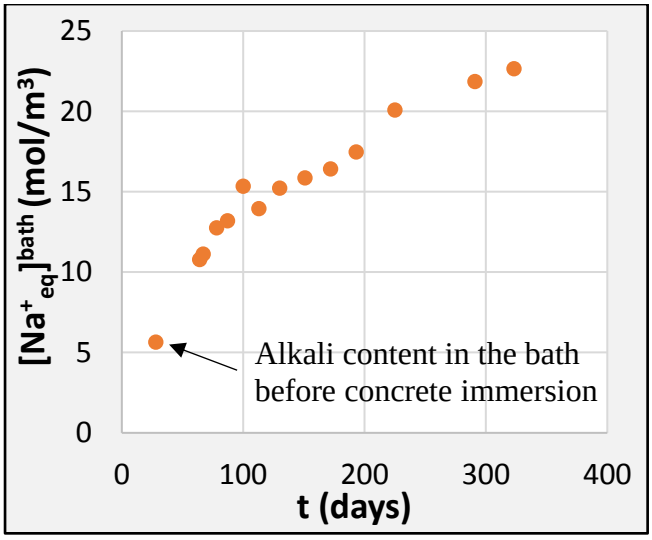

Figure 2. Alkali content evolution in storage water bath.

Alkali leaching is important data to be considered for modelling of DEF affected materials, especially regarding chemical conditions of ettringite precipitation in the cement matrix.

2.3 Experimental set-up

Prismatic specimens (100×100×500 mm) were used to analyse the impact of reinforcements and stresses on concrete subject to DEF expansion. Specimen dimensions were chosen to obtain relevant results on concrete containing 12.5 mm aggregates. **Figure 3** presents the plain specimens and the specimens reinforced in one or three directions. These specimens were subjected to the heat treatment described in 2.2 and immersed in water in order to induce delayed ettringite formation, as described in **Table 3**.

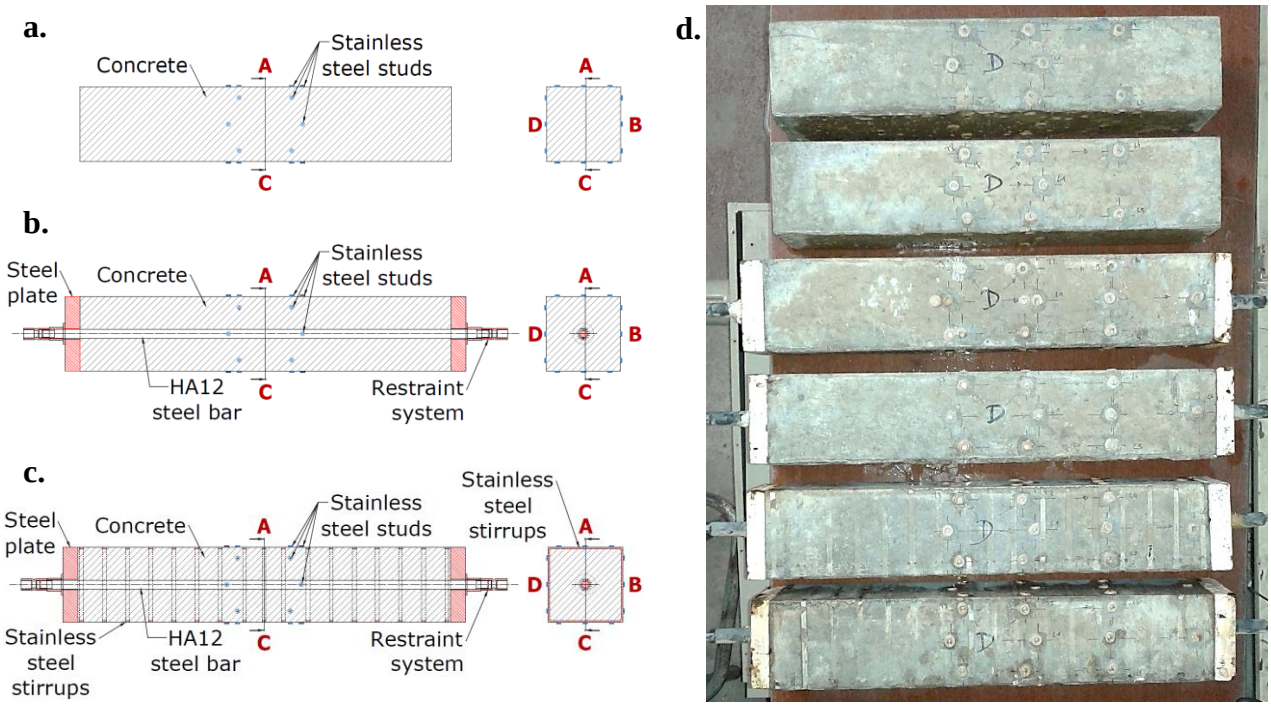

Figure 3. Non-reinforced (**a.**), axially reinforced (**b.**) and triaxially reinforced (**c.**) specimens (100×100×500 mm).

Table 3. Designation of concrete specimens (*Nb = number of specimens*).

Designation	Nb	Geometry (mm)	T_{max} during the cure	Conservation	Axial bars	Transverse stirrups	Axial pre-stressing
20 °C-28d	7	φ110×220	≈ 20 °C	Storage RH 50%	-	-	0
80 °C-28d	7	φ110×220	T_{max} = 80 °C	Storage RH 50%	-	-	0
20 °C-333d	7	φ110×220	≈ 20 °C	Immersed	-	-	0
80 °C-333d	7	φ110×220	T_{max} = 80 °C	Immersed	-	-	0
Plain	2	100×100×500	T_{max} = 80 °C	Immersed	-	-	0
R[1.1%]	2	100×100×500	T_{max} = 80 °C	Immersed	HA12	-	0
R[1.1%] +S[0.7%]	2	100×100×500	T_{max} = 80 °C	Immersed	HA12	17 stirrups 5*2 mm	0
L14.5	2	100×100×250	T_{max} = 80 °C	Immersed		-	14.5 MPa

Stress-free concrete expansions were measured on plain prismatic specimens (***Plain*, Figure 3-a**). Specimens with HA12 longitudinal reinforcement (***R[1.1%]*, Figure 3-b**) were cast so that expansion under uniaxial restraint due to an internal reinforcement ratio of 1.14% could be analysed. Regular steel was used for longitudinal restraint because concrete coating was larger enough to prevent corrosion. The third type of specimens were reinforced with longitudinal bars and transversal stirrups (***R[1.1%]+S[0.7%]***, **Figure 3-c)** in order to study the effect of triaxial restraint on DEF expansion. The ratio of the transversal sections between stirrups and concrete was 0.68%. In the last two cases, steel plates (thickness 20 mm) and restraint systems were placed on both tips of the specimens in order to ensure perfect anchoring of the longitudinal bars and to homogenise longitudinal stress in the concrete. Anchor design are detailed in **Figure 4**. The ends of longitudinal steel bar were threaded and locknuts were bolted on them to completely avoid steel plate displacement during concrete swelling. Protections against corrosion were provided by heat-shrink tubes and silicone seals. Play could have remained between steel plates and concrete due to not perfectly planar surfaces and to corrosion protection application (silicone seal might have been pushed between concrete and steel plates). Moreover, play might have been worsen by concrete shrinkage. In the transversal directions, the stirrups were spread along the specimens in such a way as to obtain a significant transversal restraint on the one hand and, on the other, a sufficient contact area between the concrete and the storage water to allow alkali leaching. They were placed on the skin of the specimens to maximize the volume of restrained concrete. As there was no concrete coating to protect them from corrosion, stainless steel has been used.

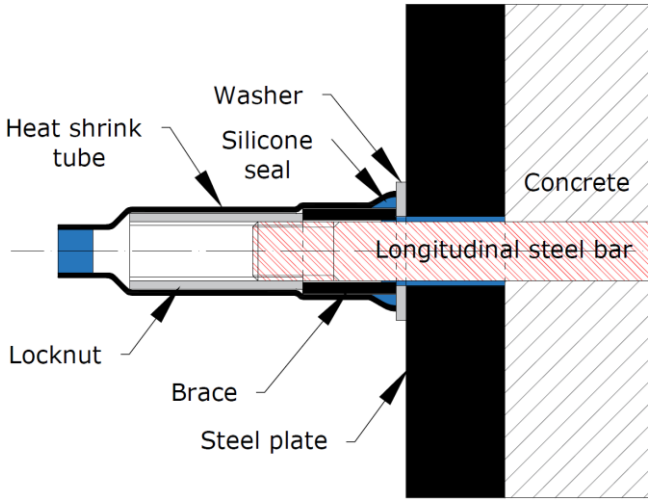

Figure 4. Longitudinal anchoring of uniaxially (***R[1.1%]***) and triaxially (***R[1.1%]+S[0.7%]***) reinforced specimens.

The specific case of uniaxial prestressed concrete (***L14.5***) is presented in **Figure 5**. The compressive stress level was equal to 14.5 MPa. It was established to supplement previous literature results [8] and to match the behaviour of real prestressed structures. The hydraulic system was composed of two actuators (a pump and a nitrogen accumulator), one for each specimen. Thus, the applied load was maintained constant whatever the concrete strain (expansion or creep) and the resulting piston displacement. Pressure in the hydraulic system was continuously checked with a manometer. Two steel plates 100×100×20 mm were placed on both part of each concrete specimens to allow stresses diffusion. Strain gauges were placed on each steel threaded rod in order to estimate its tensile stress. The weekly monitoring confirmed that the applied load was maintained constant throughout the monitoring of the specimens monitoring. Prestressed specimens were loaded 27 days after casting and immersed 24 hours later, in order to prevent transient thermal creep effects [35].

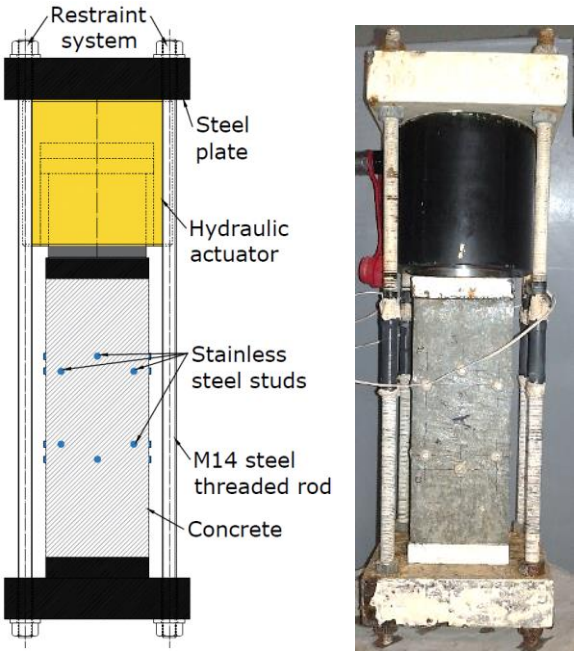

Figure 5. Specimens prestressed at 14.5 MPa.

2.4 Strain measurement

The aim was to measure the specimen expansion in the three directions and on each face. Measurements were performed with an extensometer between stainless steel studs glued on the central part of concrete surface. The measurement length was 100 mm. Before each measurement, the immersed heating resistor used to heat the storage water in the bath was switched off in order to cooled specimens from 38 °C to 20 °C in 24 hours. This process was applied to prevent thermal dilatation effects when the specimens were taken out from the bath: on the one hand, strains measurements could have impacted by the duration needed to measure and, on the other hand, thermal gradients between

specimen's skin and core could have induced concrete cracking. Cracking patterns were controlled after each expansion measurements. The specimen width was exactly equal to the measurement length. However, it was not possible to glue the steel studs onto the specimen surface in order to obtain the transversal deformation directly. Therefore, three measurements were made on each face: one along the longitudinal direction (L1 in **Figure 6**) and two along directions forming angles of 45° and 135° with the longitudinal direction (T2 and T3, respectively, in **Figure 6**). Longitudinal and transversal strains could thus be assessed from **Equation 1**, where ε_1, ε_2 and ε_3 refer to the three strain measurements made along the three directions (**Figure 6**). It is important to note that transversal strains were assessed directly from longitudinal ones. Errors were consequently added.

$$\begin{cases} \varepsilon_1 = \varepsilon_{lg}\cos^2\Phi_1 + \varepsilon_{tr}\sin^2\Phi_1 + \gamma\sin\Phi_1\cos\Phi_1 \\ \varepsilon_2 = \varepsilon_{lg}\cos^2\Phi_2 + \varepsilon_{tr}\sin^2\Phi_2 + \gamma\sin\Phi_2\cos\Phi_2 \\ \varepsilon_3 = \varepsilon_{lg}\cos^2\Phi_3 + \varepsilon_{tr}\sin^2\Phi_3 + \gamma\sin\Phi_3\cos\Phi_3 \end{cases} \Rightarrow \begin{cases} \varepsilon_{lg} = \varepsilon_1 \\ \varepsilon_{tr} = \varepsilon_2 + \varepsilon_3 - \varepsilon_1 \end{cases} \quad \textbf{Equation 1.}$$

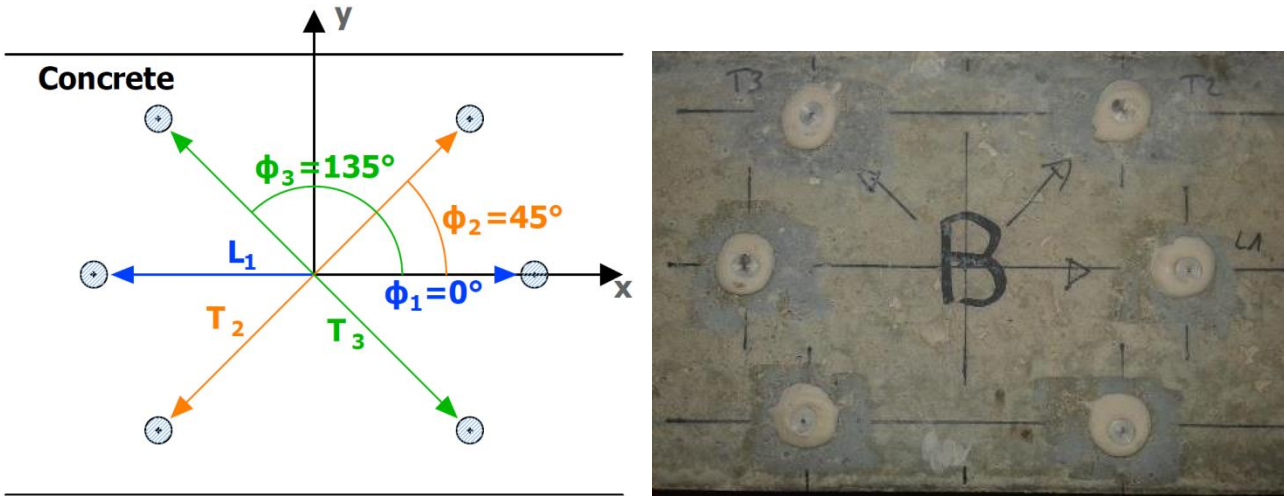

Figure 6. Orientations of strain measurements on concrete surface.

2.5 Characterization of materials

2.5.1 Longitudinal steel bars

The steel bars used for longitudinal restraint purpose were of the type usually employed for reinforced concrete (**Figure 7**). Tensile tests were performed on two similar HA12 steel bars. Stress evolution is plotted versus strain in **Figure 8**. Strain measurements were interrupted before failure because of the sensor range limits but the tests were performed until failure to obtain the ultimate strength. The Young's modulus, yield strength and ultimate strength of steel bars reached 220 GPa, 505 MPa and 609 MPa, respectively.

Figure 7. HA12 steel bar.

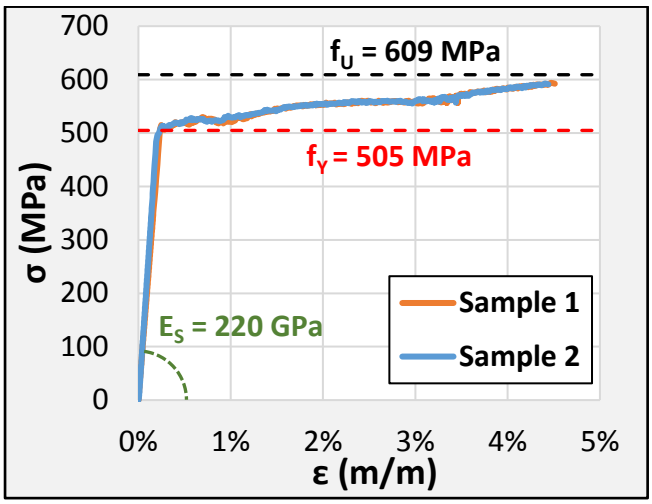

Figure 8. Experimental behaviour of steel bars.

2.5.2 Stainless steel stirrups

The stirrups were made of stainless steel (**Figure 9**).

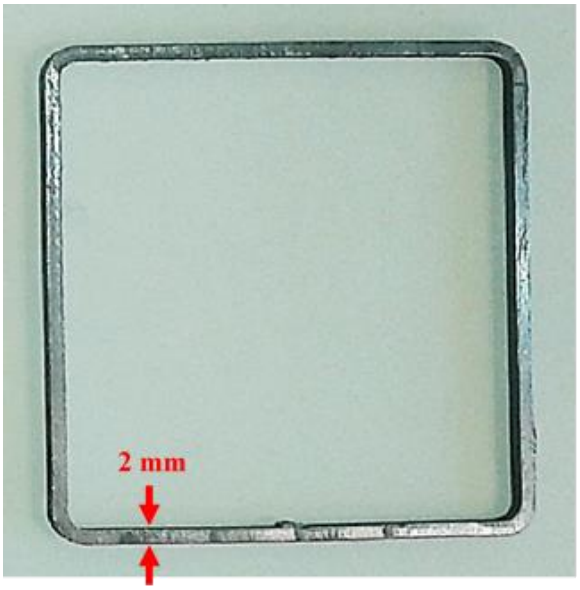

Figure 9. Stainless steel stirrup (100×100×5 mm).

Tensile tests were performed on two samples corresponding to AISI type 304 stainless steel. Stress evolution according to strain is plotted in **Figure 10**. Strain measurements were interrupted before failure because of the sensor range limits but the tests were continued until failure to obtain the ultimate strength. The Young's modulus, yield strength and ultimate strength of the steel bars reached 179 GPa, 360 MPa and 572 MPa, respectively.

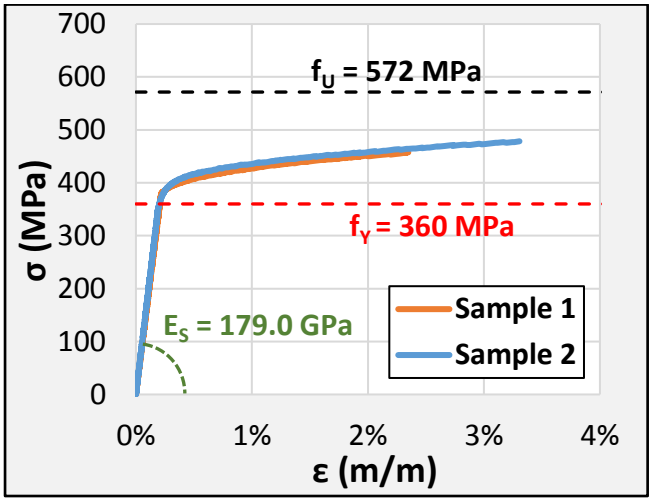

Figure 10. Experimental behaviour of stainless steel stirrups.

2.5.3 Concrete

In addition to the concrete prisms, cylindrical specimens 110 mm in diameter and 220 cm high were cast so that the mechanical behaviour of the concrete could be characterized. Young's modulus, and compressive and tensile strength were obtained, with a minimum of three tests for each. The results are presented in **Table 4**.

Table 4. Experimental Young's modulus, compression strength and tensile strength of heated and non-heated specimens.

	E (MPa)	Rc (MPa)	Rt (MPa)
20 °C-28d	40170 ± 550	40.0 ± 1.6	3.9 ± 0.4
80 °C-28d	35420 ± 270	31.3 ± 0.9	3.0 ± 0.3

The decrease of Young's modulus, between specimens subjected to heat treatment after casting and those that were not, reached 12%, while decreases in the compressive and tensile strengths were close to 22%. The hydration of the cement paste and associated species was affected by the heat treatment applied during concrete hydration and hardening. This led to a decrease in the mechanical properties

compared to non-heated specimens [36,37]. Differential thermal expansion between cement paste and aggregates may have induced damage in the Interfacial Transition Zone.

3. Experimental results

This section presents the expansions and cracking induced by DEF reactions. Phenomena observed during the first three days after specimen immersion in the storage water do not appear on figures: strain evolutions have been plotted considering time and strain values equal to zero after three days of immersion. This slight delay was considered to get rid of expansions from strains induced by water absorption and loading (in the case of ***L14.5*** specimens), in order to focus on DEF expansion. Expansions due to water absorption at this stage were close to 0.012% for both heated and non-heated specimens. Effects on water absorption expansion of changes induced by heat treatment on concrete microstructure were not visible.

Coefficient of variation has been assessed for each kind of specimen to evaluate the variability of strain measurements on each face in relation to the mean. Assessment example applied to longitudinal strains of ***Plain*** specimens is given in **Equation 2**. The notation $\boldsymbol{\varepsilon_{lg}^{Plain\ km}}$ is associated to longitudinal strain measured on the "m" face (it could be A, B, C or D) of the "k" Plain specimen (it could be 1 or 2). In all this paper, numbers "1" and "2" refer to different specimens subjected to the same restraint conditions.

$$\boldsymbol{CV_{lg} = \frac{\sigma_{lg}}{\mu_{lg}} \quad where \quad \begin{cases} \sigma_{lg} = \left(\frac{1}{8} \times \sum_{k=1}^{2}\left(\sum_{m=A}^{D}\left(\left(\varepsilon_{lg}^{Plain\ km} - \mu_{lg}^{Plain}\right)^2\right)\right)\right)^{0.5} \\ \mu_{lg} = \left(\frac{1}{8} \times \sum_{k=1}^{2}\left(\sum_{m=A}^{D}\left(\varepsilon_{lg}^{Plain\ km}\right)\right)\right) \end{cases}} \qquad \textbf{Equation 2.}$$

3.1 Expansion of the specimens

For each specimen, the strains plotted on **Figure 11** are the mean of four longitudinal measurements (one on each face of the specimens) and eight transversal measurements (two on each face of the specimens). Scatter on the measurements is reported by the minimum and the maximum values. Mean, minimum and maximum values of the expansion of each specimen are listed in **Table 5**. The time of immersion of the specimens is taken as the abscissa origin (t = 0 day). At the end of the immersion, the final longitudinal and transversal expansions due to DEF on stress-free specimens (***Plain***) are

respectively 0.59% and 0.66% (**Figure 11-a.**). Expansions in the two stress-free transversal directions are similar (coefficient of variation lower than 5%). Results show considerable scatter, lower in the longitudinal than in the transversal direction, with coefficients of variation of around 8% and 21%, respectively. Nevertheless, the mean expansion value is closer to the minimum value than to the maximum, meaning that only few values are responsible for the positive scattering. Longitudinal strains are almost equal to transversal ones, highlighting the isotropic behaviour of DEF expansion in stress-free conditions as already observed by Bouzabata et al. [8,31].

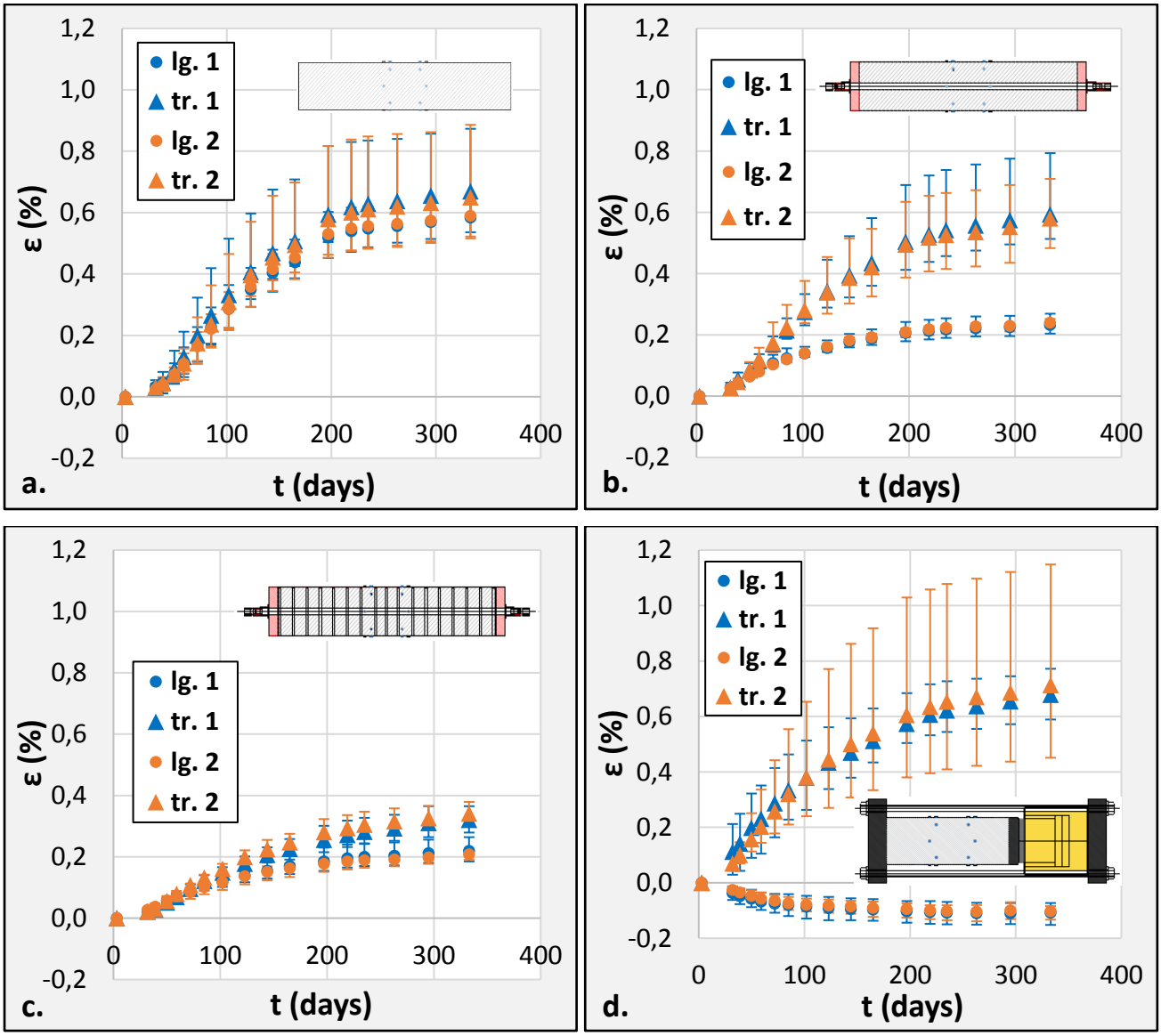

Figure 11. Longitudinal and transversal strains of plain (**a.**) uniaxially restrained (**b.**) triaxially restrained (**c.**) and prestressed under 14.5 MPa (**d.**) specimens.

Specimens under uniaxial restraint (***R[1.1%]***) exhibit longitudinal expansions of less than 0.24% (**Figure 11-b.**), with a mean coefficient of variation close to 8%. Transversal strains are more than twice the longitudinal ones, reaching 0.59%. Given the value of coefficient of variation equal to 18%,

scatter is still high in this direction compared to the longitudinal one. In this case as well, the mean expansion value is closer to the minimal value than to the maximal, meaning that only few values are responsible of the positive scattering. Expansions in the two stress-free transversal directions are similar (mean coefficient of variation lower than 4%).

Longitudinal and transversal expansion of specimens subjected to triaxial restraint (***R[1.1%]+S[0.7%]***) reach 0.21% and 0.33% respectively (**Figure 11-c.**). Longitudinal scatter is large relative to the strain values reached (coefficient of variation equal to 12%), even though the presence of stirrups seems to decrease the coefficient of variation between faces in transversal directions (10%). Once again, expansions in the two stress-free transversal directions are similar (coefficient of variation around 5%).

The longitudinal and transversal strains of prestressed specimens (***L14.5***) are plotted in **Figure 11-d**. Elastic strains are not presented on this figure in order to focus on delayed strains. Prestressed specimen strains after three days of immersion have been taken as reference to plot this figure, as it has been done for others specimens. The mean negative elastic strains measured in longitudinal directions on both loaded specimens were 0.040% and 0.042%. In the loaded direction, strains are negative and around -0.11% after 333 days of immersion. The ratio between cumulated delayed strains from loading to the end of the monitoring and elastic strains measured immediately after loading is close to 4. According to Eurocode 2 [38], this value corresponds to large creep (a ratio close to 2 can be considered as common creep). Despite a mean coefficient of variation close to 26%, the strain slopes remain negative or equal to zero throughout the monitoring: no apparent expansion seems to occur in the loaded direction. Creep exceeds DEF induced expansion occurring in the material. Strains are close to 0.70% in stress-free directions. For one of the two loaded specimens, scatter is very high in the transversal direction as well (coefficient of variation equal to 39%), even though the expansions in the two stress-free transversal directions are broadly similar (mean coefficient of variation around 4%). Once again, according to the position of the mean expansion value, a few values can explain this observed scatter.

Table 5. Mean, minimum, maximum and coefficient of variation (**CV**) values of longitudinal and transversal strains of each specimens.

Specimens	$\varepsilon_{lg}^{\infty}$				$\varepsilon_{tr}^{\infty}$			
	mean	**min.**	**max.**	**CV**	**mean**	**min.**	**max.**	**CV**

Plain 1	0.584%	-0.048%	+0.059%	6.8%	0.669%	-0.091%	+0.204%	17.8%
Plain 2	0.589%	-0.067%	+0.066%	9.0%	0.650%	-0.134%	+0.236%	21.6%
R[1.1%] 1	0.232%	-0.028%	+0.037%	10.4%	0.593%	-0.080%	+0.200%	19.6%
R[1.1%] 2	0.240%	-0.016%	+0.012%	4.2%	0.580%	-0.097%	+0.129%	14.6%
R[1.1%] +S[0.7%] 1	0.220%	-0.034%	+0.045%	15.1%	0.321%	-0.042%	+0.044%	11.6%
R[1.1%] +S[0.7%] 2	0.209%	-0.018%	+0.012%	5.3%	0.341%	-0.020%	+0.038%	6.7%
L14.5 1	-0.108%	-0.044%	+0.035%	31.5%	0.679%	-0.090%	+0.094%	9.7%
L14.5 2	-0.103%	-0.030%	+0.019%	17.7%	0.714%	-0.263%	+0.435%	38.9%

3.2 Cracking patterns

The cracking patterns described in this paragraph were observed simply with the naked eye, without optical apparatus, during the time of drying of specimens just removed from of the bath (**Figure 12**). At this moment, cracks appeared clearly visible on the concrete surface by staying dark during a longer time than the un-cracked concrete areas. Specimens in stress-free conditions (***Plain***) and with uniaxial restraint (***R[1.1%]***) exhibited the first significant cracks 120 days after immersion, when maximum strains were between 0.35% and 0.40%. They occurred mainly close to the steel plates at the extremities of the specimens. The first cracks occurred after 144 days of immersion for prestressed (***L14.5***) and triaxially restrained (***R[1.1%]+S[0.7%]***) specimens. For each specimen, the final cracking profiles (after 336 days of immersion) of the three formed faces of prisms were noted (usual defects on non-formed faces did not allow relevant mapping of cracks). Crack orientations and density are drawn in **Figure 13**.

a.

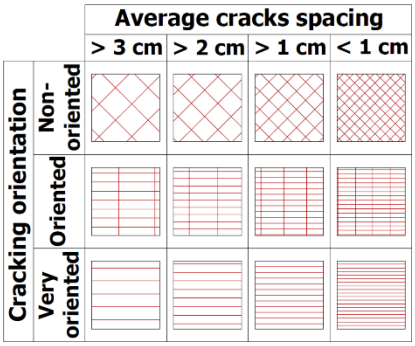

b.

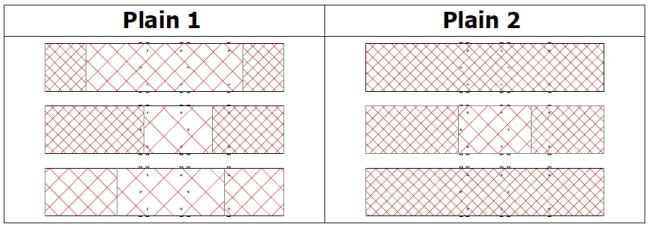

c.

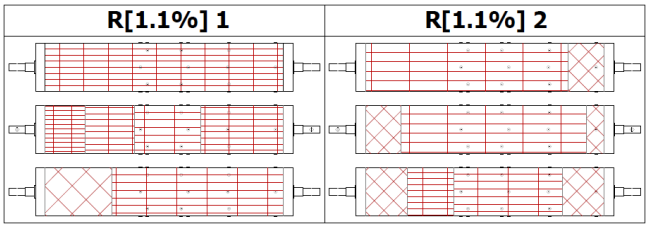

d.

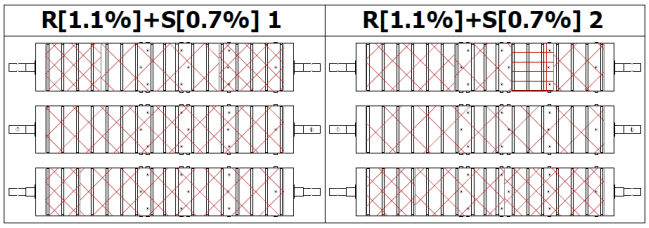

e.

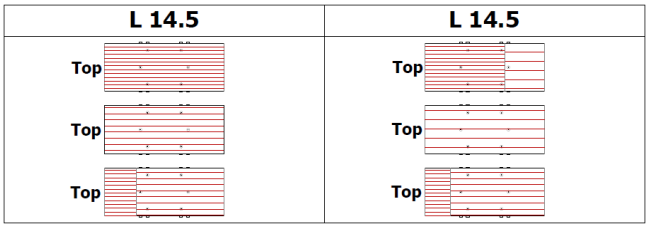

Figure 13. Orientation of cracks and density (**a.**), of plain stress-free (**b.**), of reinforced specimens (**c.**), of specimens reinforced and with stirrups (**d.**), and prestressed specimens (**e.**) after 336 days of immersion.

Figure 12. Example of cracking patterns of the specimens.

Stress-free specimens (***Plain***) exhibit dense cracking without a marked orientation. A major cracking orientation appears for specimens under uniaxial restraint (***R[1.1%]***), where most of the cracks are parallel to the direction of reinforcement. This may explain why the transversal strains are larger than the longitudinal ones. Specimens under triaxial restraint (***R[1.1%]+S[0.7%]***) present slight cracking and no marked orientation because of the effects of restraint by both bars and stirrups. Finally, prestressed specimens (***L14.5***) exhibit dense fully-oriented cracking. No transversal cracks are visible. These observations are highly consistent with the expansion monitoring, which do not pinpoint longitudinal expansion.

4. Analysis and discussion

4.1 Expansion scattering

The scatter of the experimental results has been presented in subsection **3.1**. It is mainly due to the strain measurement performed on the non-formed face, plotted A (**Figure 3)**. **Figure 14** compares the expansions measured on the non-formed and formed faces in the longitudinal (**a.**) and transversal (**b.**) directions. As confirmed by **Table 6**, the effect is more important in the transversal stress-free direction than in the longitudinal direction.

Among the possible causes of scatter between formed and non-formed faces, alkali leaching could have occurred faster on non-formed faces because of a larger, more connected porosity on this face leading to faster swelling than in the other parts of the specimen. Coefficients of variation obtained with and without non-formed face are confronted in **Table 7**. In the first case, the mean coefficients of variation in the longitudinal and transversal directions are close to 13% and 18%, respectively, while they are close to 11% and 9%, respectively, when only formed faces are taken into account. Brunetaud obtained a mean coefficient of variation close to 7% with measurements made only on formed faces

(cylindrical specimens) [24]. This value reached 10% in Martin's [27] and Bouzabata et al.'s [8,27]experiments.

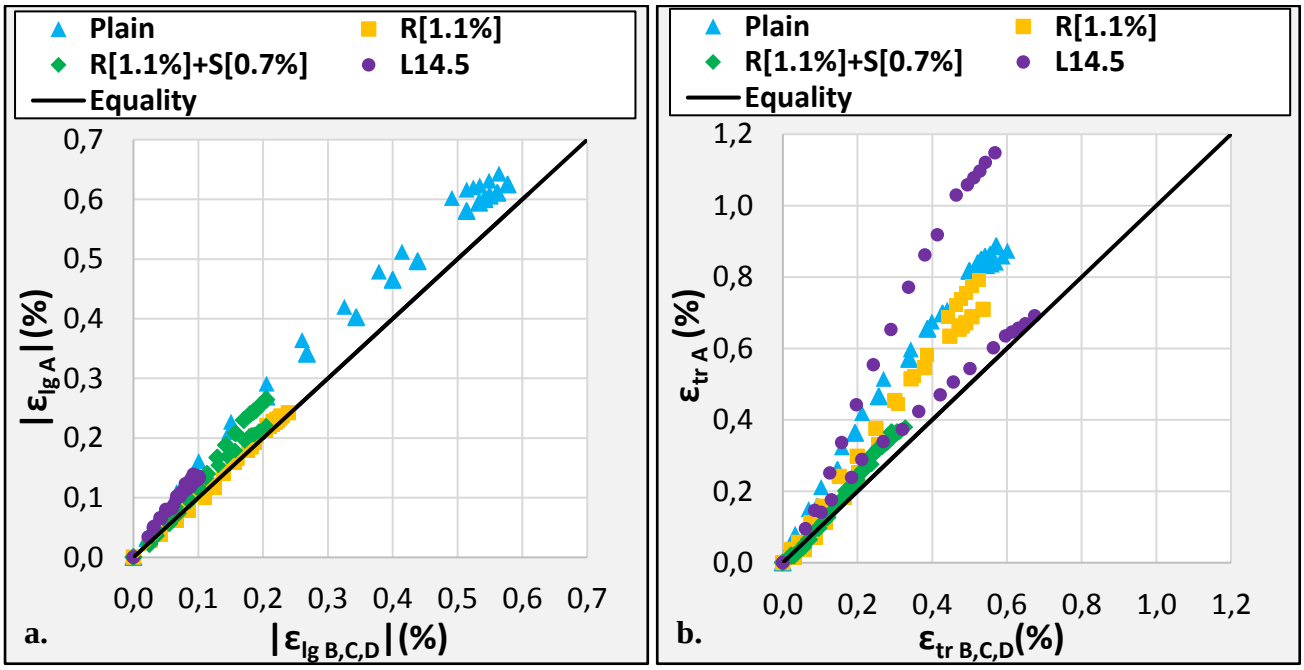

Figure 14. Non-formed face expansions (A) versus formed face expansion mean (B, C, D) for longitudinal expansion (**a.**) and transversal expansion (**b.**) (two specimens of each type).

Table 6. Ratio between non-formed face final expansions (A) and formed faces final expansion mean (B, C, D) in the longitudinal and transversal directions.

Specimens	$\frac{\lvert\varepsilon_{lg\ A}\rvert}{\lvert\varepsilon_{lg\ B,C,D}\rvert}$	$\frac{\lvert\varepsilon_{tr\ A}\rvert}{\lvert\varepsilon_{tr\ B,C,D}\rvert}$
Plain 1	1.14	1.45
Plain 2	1.08	1.55
R[1.1%] 1	1.03	1.51
R[1.1%] 2	1.01	1.32
R[1.1%]+S[0.7%] 1	1.29	1.19
R[1.1%]+S[0.7%] 2	1.07	1.15
L14.5 1	1.30	1.02
L14.5 2	1.43	2.02

Table 7. Mean and coefficient of variation (**CV**) values of longitudinal and transversal strains of each specimen.

Specimens	With non-formed face A				Without non-formed face A			
	$\varepsilon_{lg}^{\infty}$		$\varepsilon_{tr}^{\infty}$		$\varepsilon_{lg}^{\infty}$		$\varepsilon_{tr}^{\infty}$	
	mean	**CV**	**mean**	**CV**	**mean**	**CV**	**mean**	**CV**
Plain 1	0.584%	6.8%	0.669%	17.8%	0.564%	4.2%	0.601%	3.7%
Plain 2	0.589%	9.0%	0.650%	21.6%	0.577%	9.8%	0.571%	7.1%
R[1.1%] 1	0.232%	10.4%	0.593%	19.6%	0.231%	12.0%	0.527%	3.1%
R[1.1%] 2	0.240%	4.2%	0.580%	14.6%	0.239%	4.8%	0.537%	8.7%
R[1.1%] +S[0.7%] 1	0.220%	15.1%	0.321%	11.6%	0.205%	11.9%	0.306%	10.1%
R[1.1%] +S[0.7%] 2	0.209%	5.3%	0.341%	6.7%	0.205%	4.9%	0.329%	2.5%
L14.5 1	-0.108%	31.5%	0.679%	9.7%	-0.101%	36.1%	0.674%	11.2%
L14.5 2	-0.103%	17.7%	0.714%	38.9%	-0.093%	7.9%	0.569%	24.1%

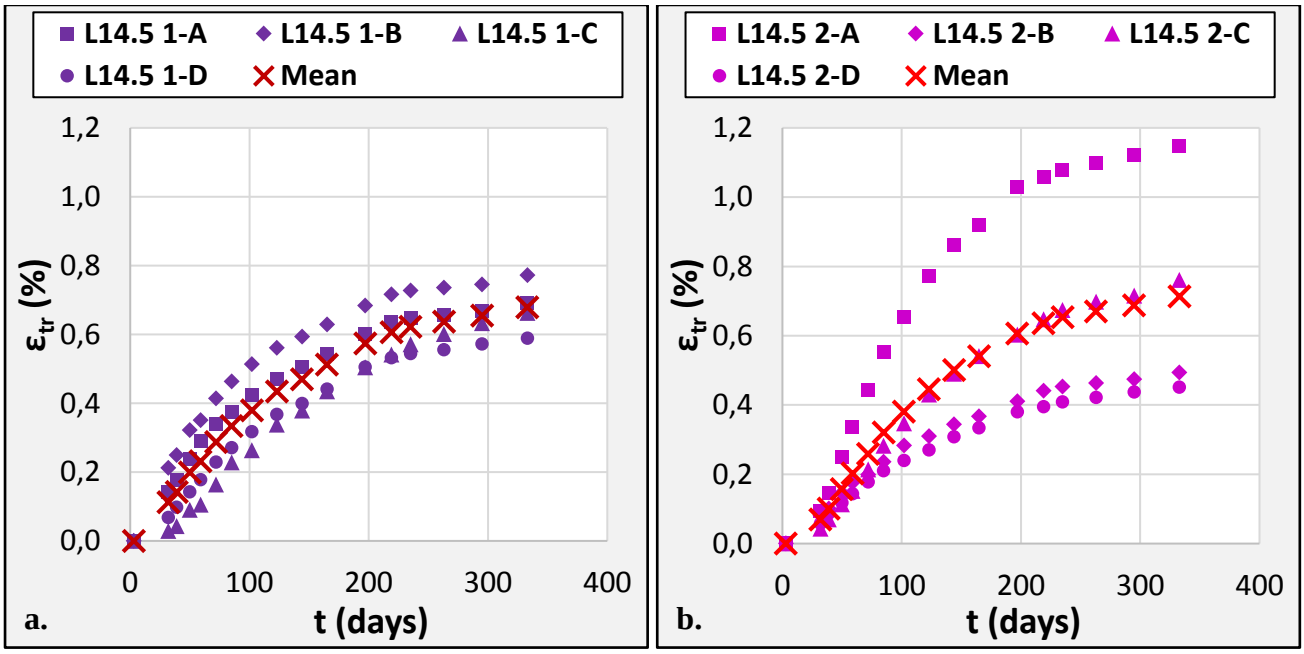

Figure 15. Transversal strains obtained on each face of the first prestressed specimen (**a.**) and of the second prestressed specimen (**b.**) (A = non-formed face; B, C and D = formed faces).

Finally, **Figure 15** highlights the random nature of the scattering phenomenon. It focuses on the specific case of the two prestressed specimens, subjected to the same thermal, hydrological and mechanical conditions. Both specimens present the same mean strains but clearly different localizations of expansion: transversal strains on the non-formed face are twice the strains measured on the formed faces for ***L14.5 2***, while they remain similar for ***L14.5 1*** (**Figure 15)**. This phenomenon might be due to a slightly dissymmetry of the loading inducing flexion.

4.2 Longitudinal strains

Figure 16 compares longitudinal strains measured on stress-free (***Plain***), uniaxially restrained (***R[1.1%]***), triaxially restrained (***R[1.1%]+S[0.7%]***) and prestressed (***L14.5***) specimens. The major effect of stress and restraint on strains development is clearly illustrated: expansions in stress-free conditions fall from 0.59% to 0.22% on restrained specimens and strains become negative for prestressing at 14.5 MPa. In the longitudinal direction, the two reinforced specimens present the same longitudinal restraint effect in spite of the presence of the stirrups in the second case. The longitudinal reinforcement effect is almost equivalent for ***R[1.1%]*** and ***R[1.1%]+S[0.7%]*** specimens: expansions reach 0.24% in uniaxially restrained specimens versus 0.21% when transversal stirrups are additionally used. Finally, a 14.5 MPa prestressing load, corresponding to 46% of concrete compression strength after heat treatment, significantly reduced concrete DEF expansion of the ***L14.5*** specimens in the loaded direction and only creep effects are visible.

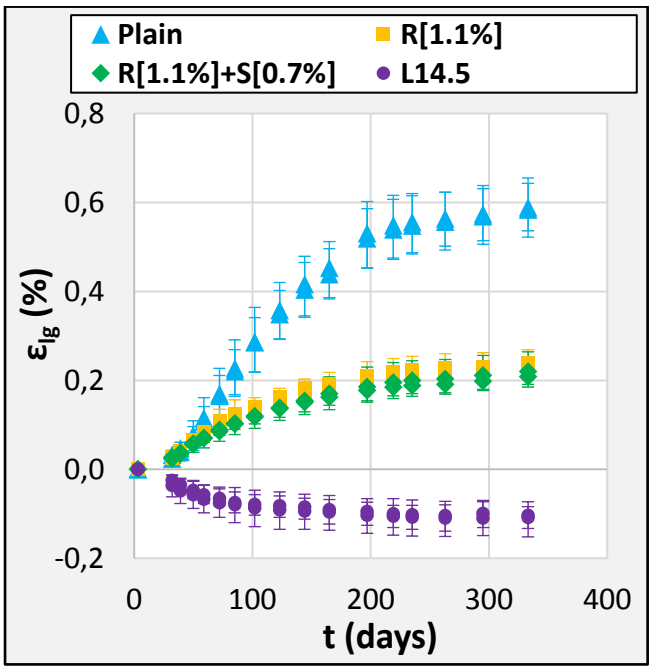

Figure 16. Longitudinal strains for all the specimens.

4.3 Transversal strains

Figure 17 compares the transversal strains measured on stress-free (***Plain***), uniaxially restrained (***R[1.1%]***), triaxially restrained (***R[1.1%]+S[0.7%]***), and prestressed (***L14.5***) specimens. Longitudinal restraint or loading have no major impact on transversal strains. No transfer of strain from the restrained direction to the others is observable when comparing results for ***R[1.1%]*** and ***Plain***. Final transversal expansions are even slightly lower when restraint is applied, reaching 0.59% instead of 0.66% in stress-free conditions. This reduction appears to be progressive from immersion to the stabilization of expansions. The comparison between the mean transversal strains obtained on the prestressed specimens ***L14.5***, equal to 0.70%, and on the stress free specimens (***Plain***) seems to confirm the absence of DEF expansion transfer in the case of uniaxial external loading, even though scatter remains high. The difference of positive strain between ***Plain*** and ***L14.5*** specimens is closed to 460 µm/m, which remains higher than Poisson effect regarding creep (positive strain of prestressed specimens should be increased of about 220 µm/m, assuming a Poisson's coefficient equal to 0.2 and negative strain due to creep close to -0.11%). As expected, the main difference is noted when stainless steel stirrups limit transversal expansions (***R[1.1%]+S[0.7%]***) from 0.66% to only 0.33%.

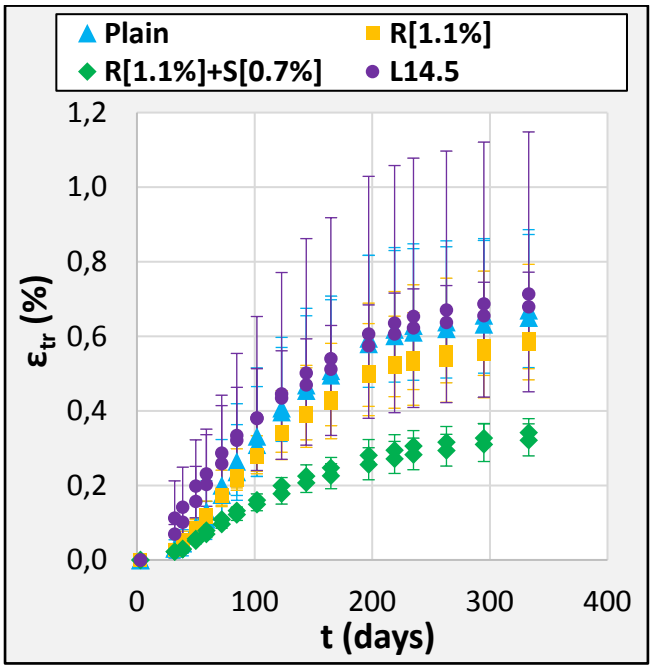

Figure 17. Transversal strains for all the specimens.

4.4 Volumetric strain and strain transfer

The relative volumetric strain is defined as the change in volume divided by the original volume. **Equation 3** expresses how it is assessed:

$$\frac{\Delta V}{V_0} = (1 + \varepsilon_{xx})(1 + \varepsilon_{yy})(1 + \varepsilon_{zz}) - 1 \approx tr(\varepsilon) \qquad \textbf{Equation 3.}$$

The presence of the restraint induces a decrease of the associated specimen volumetric strain, as highlighted by **Figure 18**. The volumetric strain for stress-free specimens (***Plain***) reaches 1.92% after 333 days of immersion. It is only 1.42% (decrease of about 26%) and 1.29% (decrease of about 33%), respectively, for uniaxially reinforced (***R[1.1%]***) and prestressed (***L14.5***) specimens, and falls to 0.88% (decrease of about 54%) when specimens are triaxially restrained (***R[1.1%]+S[0.7%]***).

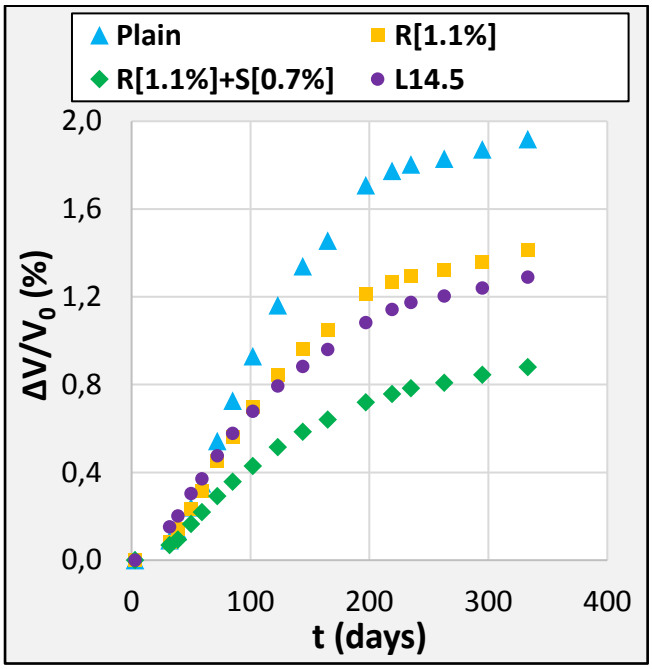

Figure 18. Volumetric strains for all the specimens.

Mechanical loading could have impacted the chemical reactions in the cement matrix. Even though the transversal expansions show that the reaction kinetics is not modified by restraint or stress, under loading, the volume of delayed ettringite formed could be lower than in stress-free conditions. Based on thermodynamic statements, Correns' law gives a logarithmic relation between the pressure acting on crystal and its relative solubility [39]. This relation indicates that the crystal solubility raises with the mechanical pressure applied directly on it. In the case of DEF in concrete, pressure on crystals is applied by the pore wall [40]. If the pressure needed to stop crystal growth in a supersaturated solution generates higher local stress than the local tensile strength of the matrix, cracks might appear. Local poral pressure then decreases because of this voids creation, and so does the ettringite solubility. Consequently, new ettringite crystals could precipitate in these voids without major effects on strains. Supersaturation in the poral solution decreases until thermodynamic equilibrium is reached.

Mechanical loading does not directly act on crystals but on the matrix. Consequently, matrix cracking is avoided in perpendicular directions regarding loading direction. In the case of triaxially restrained DEF reactive concrete, pressure acting on crystal might be largely higher than in unloaded concrete because the matrix cracking is delayed. Thus, ettringite solubility might remain higher and thermodynamic equilibrium could be reached forming less ettringite. Nevertheless, the pressure necessary to impact ettringite solubility seems difficult to assess and literature results are too scattered to conclude on this point. Consequently, this phenomenon could contribute to the volumetric strain decrease of restrained specimens (***R[1.1%]+S[0.7%]***), but is not necessarily the only or even the main one. According to Scherer, there is a competition between ettringite crystallization in nanopores and in macropores [40]. The first phenomenon (crystallization in nanopores) is due to supersaturation resulting from primary hydrates dissolution and leads to high crystallization pressure inducing cracking and thus expansions. Massive crystal morphology is associated to these pressures [11,41–43]. It can be concluded that ettringite precipitates in massive form when its growth is restrained. In restrained concrete, pressure acting on crystals can be higher than in stress-free conditions: ettringite presenting a higher density could thus be formed and might explain the decreases of volumetric strains between stress-free and restrained or loaded specimens. The second one (crystallization in macropores) might be induced by nanocrystals dissolution and transfer to larger crystals. It could be the consequence of the relation between ettringite solubility and applied pressure given by the Correns' law. Scherer suggests that the diffusion kinetics of ions in the matrix could last weeks. Finally, the mechanical loading could raise the solubility of ettringite nanocrystals and increase the fraction of the delayed ettringite volume that would precipitate in the initial porosity without causing supplementary porous pressure.

To conclude, all of these phenomena imply a relation between the poral pressure and the volume occupied by ettringite, whether it be due to the quantity of delayed ettringite formed, through its solubility, or to the occupied volume, through its morphology. The cases of uniaxially restrained specimens (***R[1.1%]*** and ***L14.5***) question the sufficiency of these assumptions because matrix cracking is not delayed in the unrestrained directions, limiting poral pressure increase. These questions are fundamental and have to be investigated through numerical modelling or a dedicated experimental plan. These results will be discussed and compared with the literature in subsection **4.7**.

4.5 Anisotropy

Longitudinal strains are plotted versus transversal strains in **Figure 19.a**. Below 0.1% of expansion, behaviour of all kinds of specimen is very similar. In reinforced specimens, the necessary expansion to obtain significant stress in steel bar (and thus in concrete) depends on bonding conditions. Steel bar contribution probably does not start simultaneously with expansion because of the remaining play between steel plates and concrete. It can also depend on the state of the interface between bar and concrete. Thus, influence of restraint on strains is progressive and first expansions certainly take place in close to stress-free conditions. Consequently, the anisotropy coefficient is defined in each case as the slope of the curve of longitudinal versus transversal strain between 0.1% and final expansion. These coefficients are given in **Table 8**. Curve slope evolution is plotted as a function of associated longitudinal strains in **Figure 19.b**.

Stress-free specimens (***Plain***) show fairly isotropic behaviour, longitudinal expansion being lower than transversal expansion with a coefficient close to 0.88. Slope of the longitudinal - transversal strains curve remains close to this value all along the monitoring. This statement could be related to the measurement procedure: strains were measured on concrete surfaces instead of being measured between specimens opposite surfaces. Nevertheless, Bouzabata et al. observed the same kind of behaviour in mortar prisms, measuring strains between specimen's opposite surfaces [8]. This moderate anisotropy remains usual given the discrepancy among DEF expansions in stress-free conditions. Uniaxially restrained specimens (***R[1.1%]***) had more anisotropic behaviour, with an average coefficient close to 0.33. This leads to the conclusion that, even if DEF expansion is isotropic under stress-free conditions, the expansions induced by DEF under restraint conditions become anisotropic. This can be explained by the cracking orientation induced by the local equilibrium between the tensile stress due to the pressure caused by the new products and the compressive stress induced by the expansion restraint, as described for the case of Alkali-Silica Reaction in [44]. Anisotropic behaviour seems to be related with longitudinal strains from immersion to the end of the monitoring. The more the longitudinal strain increases, (and thus the higher the longitudinal induced stress is), the more anisotropic is the expansion. Anisotropy coefficient reaches the median value of 0.56 in the case of specimens under triaxial restraint (***R[1.1%]+S[0.7%]***). The same conclusion as for uniaxially restrained specimens can be stated in this case. On the curve of longitudinal strain plotted as a function of transversal strain (**Figure 19.a)**, the initial slope seems to be higher than 1.0, contrary to what can be observed at the end of the monitoring. This is confirmed by **Figure 19.b** and can be induced by a better anchoring of the stirrups than the longitudinal bars. Except this initial difference, slope evolution is similar to the previous one, highlighting lower transversal stress induced by stainless steel stirrups in concrete than the one induced in the longitudinal one by steel bar, as expressed below

in subsection **4.6**. To finish with, prestressed specimens (***L14.5***), not represented in the figure, exhibited the greatest anisotropy: there was no longitudinal expansion (but negative strains due to creep) and thus the anisotropy coefficient tended towards zero.

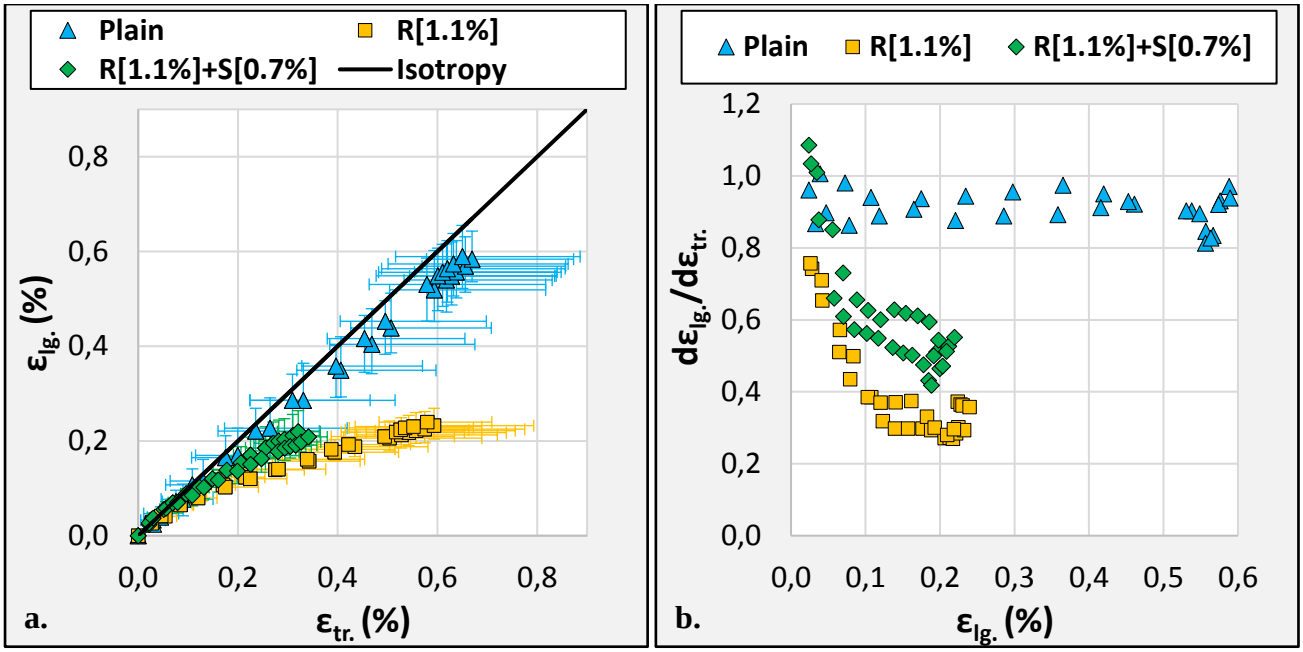

Figure 19. Longitudinal versus transversal strains of plain and restrained DEF specimens (**a.**). Slopes of these curves as a function of longitudinal strains (**b.**).

Table 8. Anisotropy coefficients of DEF expansion under restraint.

Specimen	Anisotropy coefficient
Plain 1	0.868
Plain 2	0.890
R[1.1%] 1	0.311
R[1.1%] 2	0.348
R[1.1%]+S[0.7%] 1	0.594
R[1.1%]+S[0.7%] 2	0.527

4.6 Induced stresses

Stresses in restrained specimens (***R[1.1%]*** and ***R[1.1%]+S[0.7%]***) can be assessed from strain measurements on the concrete surface. Concrete and reinforcement strains are taken to be equal in the longitudinal direction as bonding is assumed to be ensured by the steel plates placed on both extremities of the specimens (after the short period necessary to compensate the play between the concrete and the plates). This assumption is a simplification implying that the strain field is homogeneous. Longitudinal concrete stress is assessed using **Equation 5**, where S_s and S_c are respectively the steel and concrete cross sections, E_s is the steel Young's modulus of the steel, and ε_s^{pl} are the steel strains due to plasticity if the elastic limit of the steel is reached.

$$\begin{cases} \varepsilon_c = \varepsilon_s \\ S_c\sigma_c = -S_s\sigma_s \\ \sigma_s = E_s.(\varepsilon_s - \varepsilon_s^{pl}) \end{cases}$$

Equation 5.

According to this calculation, concrete longitudinal stresses reach a compression of 5.8 MPa and 5.4 MPa in specimens under uniaxial (***R[1.1%]***) and tri-axial (***R[1.1%]+S[0.7%]***) restraint, respectively, as shown in **Figure 20.a**. Loading was progressive, following strain evolutions. After 333 days of immersion, expansions are almost sufficient to plasticize the longitudinal steel bars.

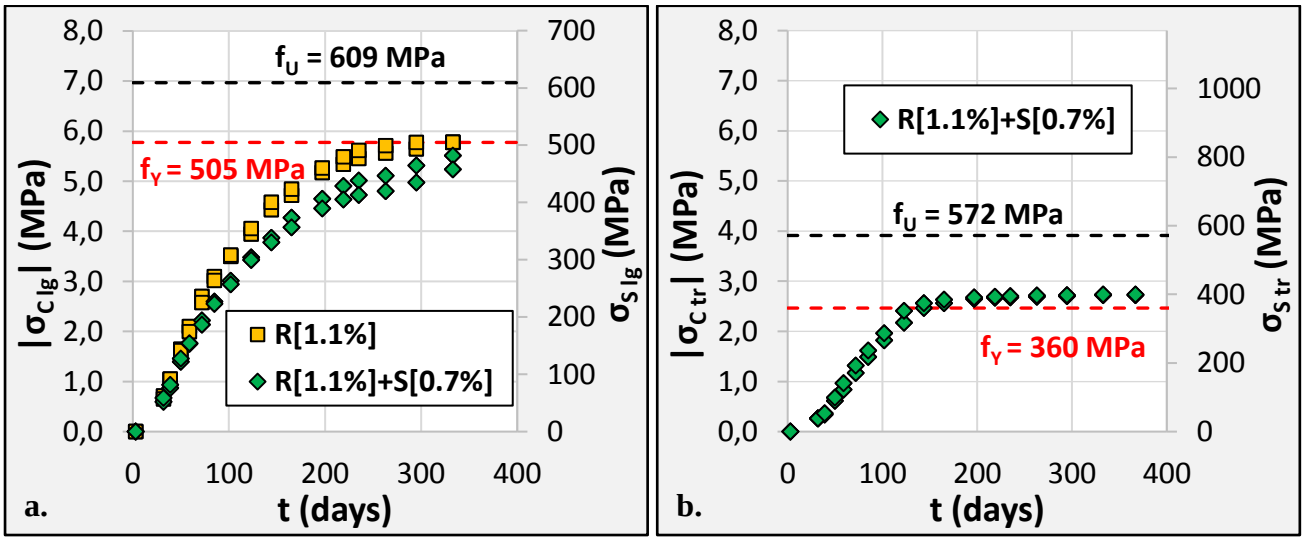

Figure 20. Longitudinal (**a.**) and transversal (**b.**) stresses induced in concrete and reinforcements/stirrups.

In the transversal direction, it is assumed that the distribution of the stirrups along the specimens (***R[1.1%]+S[0.7%]***) homogenizes strains. The calculation is similar to the one used for longitudinal stresses, except that S_s, S_c refer to transversal sections, and the values of E_s and ε_s^{pl} have to be replaced by stainless steel characteristics.

Considering **Figure 20.b**, transversal stresses reach 2.5 MPa in specimens under triaxial restraint (***R[1.1%]+S[0.7%]***). Once again, loading was progressive, following the evolutions of the strains. Throughout the monitoring, transversal stresses remain clearly below longitudinal ones because the section ratio between steel and concrete is lower in the transversal (0.7%) than in the longitudinal direction (1.1%). As shown in subsection **2.5**, steel and stainless steel have quite different behaviour when tensioned, which contribute to the divergence between the evolutions of the two stresses after 100 days of immersion. From that stage, transversal expansions are sufficient enough to plasticize stainless steel stirrups.

4.7 Comparison with the literature

4.7.1 Experimental results from the literature

Bouzabata et al. studied immersed mortar prisms (40×40×160 mm) affected by DEF under stress-free conditions and homogeneous restraint imposed by external reinforcements [8]. Two levels of restraint were imposed, depending on the diameters of the steel bars: four bars were 2 mm in diameter (***4D2***) and four had a diameter of 5 mm (***4D5***), corresponding to external reinforcement ratios of 0.8% and 4.9%. Expansions of stress-free specimens were isotropic, reaching 2.1% on average, while those of restrained prisms were anisotropic. Anisotropy coefficients, assessed from experimental raw data given in Bouzabata's paper (Figure 6.a of this reference), were around 0.30 and 0.08 respectively for the ***4D2*** and ***4D5***. The first coefficient is quite close to the one obtained above in our study (0.33 for ***R[1.1%]*** with reinforcement/concrete ratios close to 1.1%). This means that, even though in one case the material used was mortar with free expansion reaching 2.1% and external reinforcement and in the other case concrete with free expansion reaching only 0.66% of expansion in stress-free conditions and internal reinforcement, DEF expansion behaviour seems to remain similar when uniaxial restraint is applied.

Bouzabata et al. observed that transversal expansions were slightly larger for specimens under longitudinal restraint than for stress-free specimens. Nevertheless, the gap was not sufficiently large to conclude on a complete transfer of DEF expansions from loaded to free directions. The expansion measured in the stress-free direction of restrained specimens was not modified in the present study, even under uniaxial loading under 14.5 MPa (***L14.5***). Thus, as in Bouzabata et al.'s study, the final volumetric strains were impacted. As presented above, stress-free volumetric strains reached here 1.92%, with a decrease of about 26% when uniaxial restraint was applied. With a more reactive formulation and consequently over a different scale of strains (volumetric strains of about 6.1% in

stress-free conditions obtained on mortar), Bouzabata et al. observed a decrease of the volumetric strains for the uniaxially restrained specimens 4D2 (volumetric strains close 5.0%). For this material developing a larger potential of expansion, the relative decrease was about 20%.

The effects of homogeneous restraint imposed by external reinforcements on immersed mortar have also been studied on thin-walled hollow cylinders (diameter 30.0 mm, wall thickness 2.5 mm) affected by external sulfate attack by Müllauer et al. [26]. These results can be compared to DEF induced expansion because of the cylinder thickness: swelling due to external sulfate attack can be assumed homogeneous in the specimens, as it occurs in DEF affected material. Although final free expansions were more than ten times higher than those obtained in the present experimental study, the results can be compared for expansions lower than 1%. **Figure 21** presents the evolution of longitudinal stresses according to expansions in stress-free conditions for uniaxially restrained mortar specimens undergoing ESA (External Sulfate Attack) as studied by Müllauer et al. and for uniaxially reinforced concrete specimens subjected to DEF. In spite of the different conditions of restraint in terms of steel / concrete ratio, the curves aspects are very similar for the two experimental works. Up to 0.2% of free expansion, corresponding to a stress value close to 2.5 MPa, the behaviour is almost linear and similar for the two experimental works. Above 0.2% of free expansion, stresses in specimens subjected to DEF become higher than those in thin-walled specimens subjected to ESA: at 0.4%, the difference is still lower than 1 MPa but, after 0.4% of expansion, the evolution in thin-walled specimens slows significantly and the stresses are lower than 4.0 MPa for free expansion close to 0.58%, whereas stress evolutions in DEF-specimens remain almost linear, reaching 5.8 MPa for the same value of free expansion. As the restraint was lower in the present work than in Müllauer et al.'s study, lower compressive stresses could have been expected. However, this was not observed (**Figure 21**). The explanation could be found in the progressive buckling of the thin-walled cylinders. Because of their thinness, the mortar specimens studied by Müllauer et al. might have been subject to mechanical instability under compression. Some of the specimens showed typical signs of buckling ruin (barrel shape), as shown in Müllauer et al.'s paper. As a result, the decrease of stress might no longer have been representative of the evolution of the stress in the material but might have been due to external structural conditions. The specimens used in the present work were quite massive, which prevented instability mechanisms and might explain the differences of results for the two sets of experiments. To conclude, stresses induced by ettringite formation appear to be similar and to be fairly independent of the material properties in the two cases compared (at least for expansion lower than 0.4%). More

investigations are required to conclude on the existence of a common mechanical behaviour for both internal and external sulfate attacks in restraint conditions.

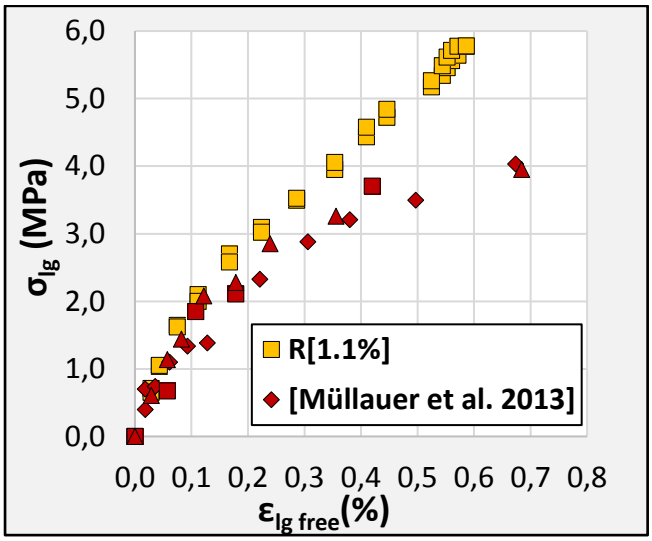

Figure 21. Longitudinal stresses evolution in restrained DEF-concrete and ESA-mortar specimens [26] according to free expansion.

4.7.2 Empirical models of restrained expansion from the literature

ASR and DEF are often compared because of their similar mechanical effects on concrete. Charlwood's empirical law, based on studies of ASR-damaged dams and plants, defines a relation between final total strains of ASR affected concrete and compressive stress in a designated direction [45]. In this law, longitudinal and transversal directions are treated independently. In **Equation 6**, $\boldsymbol{\varepsilon_I^0}$ is the stress-free expansion in direction I, $\boldsymbol{K}$ a material parameter, σ_I the compressive stress in direction I, and $\boldsymbol{\sigma_I^t}$ the stress threshold (equal to 0.3 MPa) below which stress has no impact on strain.

$$\boldsymbol{\varepsilon_I} = \begin{cases} \boldsymbol{\varepsilon_I^0} \\ \boldsymbol{\varepsilon_I^0 - K.\log\left(\frac{\sigma_I}{\sigma_I^t}\right)} \end{cases} \qquad \textbf{Equation 6.}$$

It can be conclude from sections 4.2, 4.3 and 4.4 that experimental strain in a given direction appears independent from restraint applied on others. Consequently, Charlwood's law can be applied on both directions of all the specimens. To be consistent with Charlwood's measurements method, total strains were considered. **Figure 22** confronts experimental results and Charlwood's law applied to DEF expansion, with parameter K fitted at 0.0033. The mean of longitudinal and transversal strains of stress-free ***Plain*** specimens has been taken for $\boldsymbol{\varepsilon_I^0}$.

The experimental point corresponding to 14.5 MPa was obtained by means of uniaxial prestress, unlike to the three ***R[1.1%]*** and ***R[1.1%]+S[0.7%]*** points that were uniaxially or triaxially restrained. Actually, Charlwood's law is based on the hypothesis of restrained concrete. This might explain why experimental longitudinal strains at 14.5 MPa are not well evaluated by the empirical law. In cases of restraint, stresses are induced by longitudinal strains (or transversal strains when stirrups were added). Thus, compressive stresses are equal to zero as long as DEF has not started, allowing expansion in this direction while compressive stresses are not high enough to prevent cracking perpendicular to the restraint [44]. In contrast, stresses are always equal to 14.5 MPa in prestressed specimens ***L14.5*** throughout the DEF reaction, preventing any expansion in the loaded direction.

Although it is based on ASR-damaged structures, Charlwood's law seems to be relevant to estimate DEF expansion under restraint. Assessing the needed physical input parameters for such modelling purpose remains the main limitation of this approach. For each material, a specific case of restrained expansion in which the final strains and induced stresses are known is necessary to evaluate the value of the parameter *K*. In addition, for each restraint case, the final stress-free expansion and final induced stresses must be known. Nevertheless, this law appears unusable for expansion prediction of loaded concrete elements such as prestressed concrete or bridge columns.

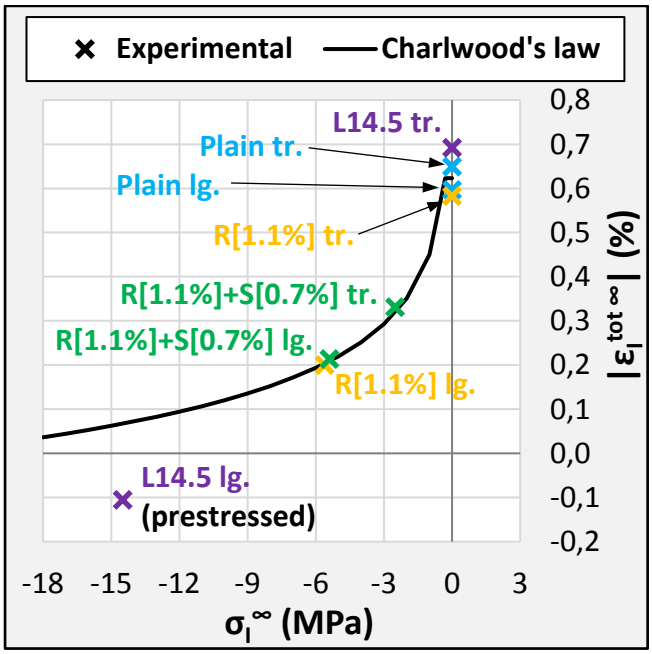

Figure 22. Comparison between experimental results and Charlwood's law applied to DEF (K = 0.0033).

A semi-empirical model for DEF expansions in reinforced and prestressed concrete based on a strain energy approach has been proposed by Karthik et al. [46,47]: the total strain energy of DEF expansion on plain concrete, U_{PC}, is considered equal to the total strain energy of DEF expansion on reinforced concrete, U_{RC}, which is composed of the strain energy of the concrete, U_C, of the steel reinforcements, U_S, of the prestressed strands, U_{PS}, and possibly of constant stress, U_{const}. The main hypotheses used are:

- The kinetics of expansion between initiation and final expansion is managed thanks to a hyperbolic tangent function given in **Equation 7**, in which $\varepsilon(t)$ is the expansion strain in reinforced concrete due to the combined effects of ASR and DEF expansion at time t; ε_ρ^{max} is the maximum expansion in concrete, assessed as a function of the reinforcement ratio, ρ; t_0 is the initiation time when expansion due to DEF starts; and t_r is the "rise time" of the tangent line to the hyperbolic curve. **Figure 23** shows the curve of stress-free expansion assessed to fit the stress-free experimental expansion. Here, the values of the initiation time t_0 and the "rise time" t_r are respectively 35 days and 125 days.

$$\varepsilon(t) = \varepsilon_\rho^{max} \times tanh\left\langle \frac{t - t_0}{t_r} \right\rangle \qquad \textbf{Equation 7.}$$

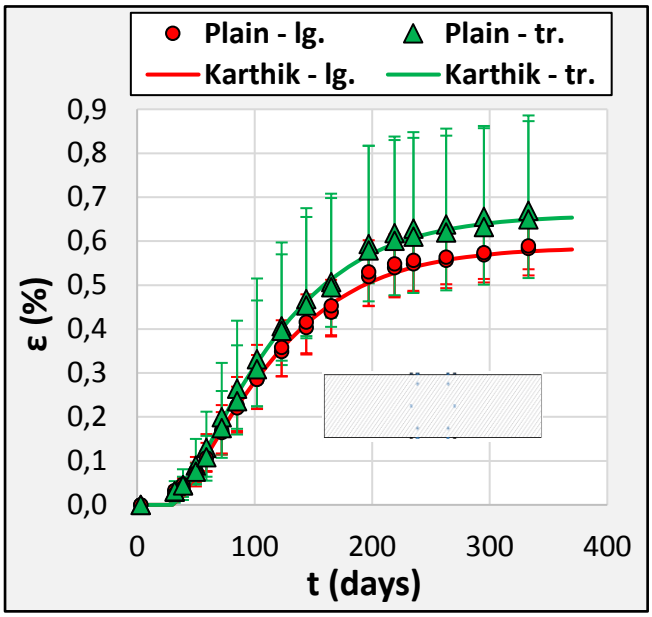

Figure 23. Stress-free expansion curve of Karthik et al.'s model fitted with stress-free experimental expansion points.

- Each direction of a reinforced concrete structure or specimen is treated independently of the others, uncoupling expansion in longitudinal and transversal directions.

- Values of the ratio, n, of steel/concrete elastic moduli, and the strain corresponding to the tensile stress of concrete, $\varepsilon' t$, have been modified as expressed in **Equation 8** to take the concrete creep effects into account.

$$n = 3 \times E_s / E_c$$
$$\varepsilon'_t = 3 \times f'_t / E_c$$

Equation 8.

Using the values of the parameters defined previously, Karthik et al.'s model is tentatively applied to uniaxially and triaxially reinforced specimens and is compared to experimental expansions in **Figure 24**.

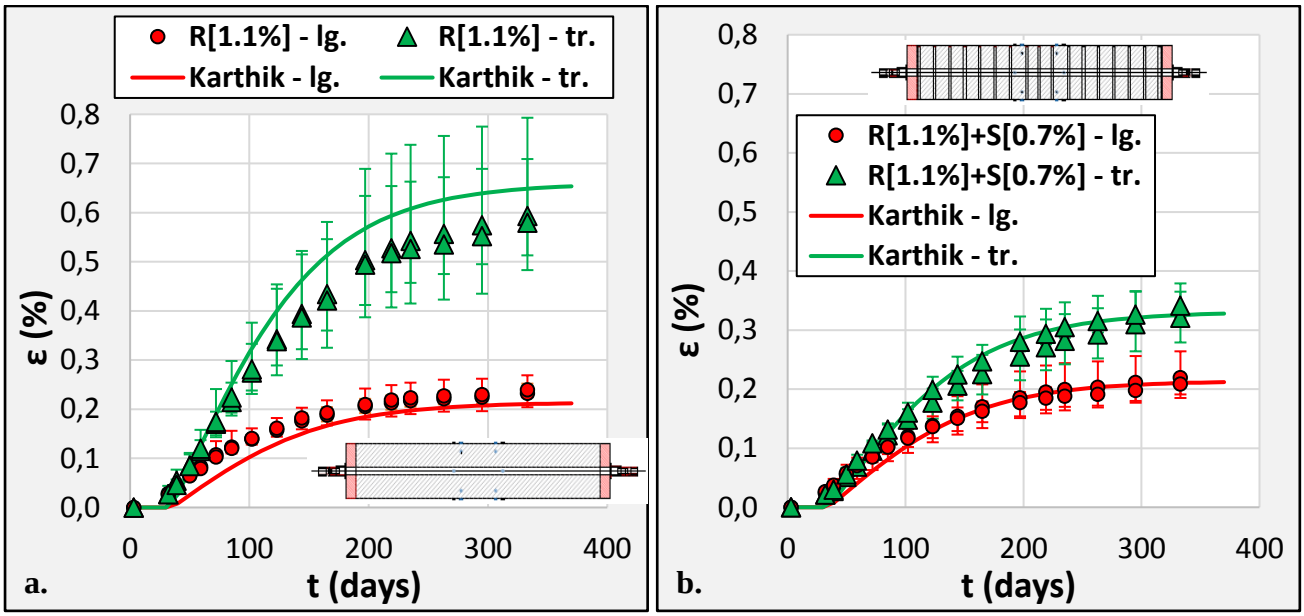

Figure 24. Comparison between experimental results and model proposed by Karthik et al. [46] for uniaxially (**a.**) and triaxially (**b.**) reinforced specimens.

This model is no longer applicable when strains are negative, which is the case in the longitudinal direction for prestressed specimens (***L14.5***); that is why it is not calculated here. For uniaxially reinforced specimens (***R[1.1%]***), expansion of the restrained direction are well assessed, although the calculated strains remain slightly below experimental ones (relative error of modelling close to 10%). In contrast, the transversal calculated strains are larger than those measured experimentally. The relative error remains sensible, below 12%. In the case of triaxially restrained specimens (***R[1.1%]+S[0.7%]***), the assessment of longitudinal and transversal strain is almost perfect, with a modelling relative error below 1% in both directions. The approximation made on the strain kinetics fits the experimental observations well. Nevertheless, longitudinal expansion kinetics appears a bit underestimated. That may have been induced by the play between the concrete and the plates observed

experimentally, which could have delayed the restraint action of the bars. The hypothesis of uncoupling resolution between longitudinal and transversal directions in the case of DEF expansion seems relevant, as seen before using Charlwood's law. Finally, this comparison is very conclusive and confirms the validity of the model for the reinforced concrete expansion assessment when a few physical input parameters are known: behaviours and geometries of materials, final stress-free expansion, and two indicative times for kinetics fitting.

5. Conclusions

The influences of both reinforcements and prestress on DEF expansion in concrete have been covered in the present work and experimental results have been compared to previous studies from the literature. Most of the conclusions drawn by Bouzabata et al. for uniaxial restraint have been extended from externally restrained mortar to internally reinforced concrete. They have also been extended for multi-axial restraint and large applied compressive stress:

- DEF expansion is isotropic in stress-free conditions (***Plain***).
- Restraint and prestress lead to a decrease of DEF expansion in the loaded direction without significant impact on the stress-free directions. Cracks appear mainly parallel to the restraint.
- Concrete prestressed under 14.5 MPa (***L14.5***) exhibits no apparent expansion in the loaded direction, but, on the contrary, negative strains due to creep. Nevertheless, DEF expansions might have occurred, hidden by creep effect.
- DEF expansion under stress is anisotropic. Anisotropy coefficients, defined in each case as the slope of the curve of longitudinal versus transversal strains, were 0.33, 0.56 and 0.00, respectively, when uniaxial restraint (***R[1.1%]***), triaxial restraint (***R[1.1%]+S[0.7%]***) or uniaxial loading under 14.5 MPa (***L14.5***) was applied.
- Volumetric strains were observed to vary: decreases of about 26%, 54% and 33% with respect to the volumetric expansion of stress-free specimens (***Plain***) were measured after 333 days of immersion for uniaxially restrained (***R[1.1%]***), triaxially restrained (***R[1.1%]+S[0.7%]***) and prestressed (***L14.5***) specimens, respectively.

Comparison with the work of Müllauer et al. showed that the correlation between the stresses induced by restraint and a given stress-free expansion was very similar, whether the cases concerned internal or external sulfate attack (at least for expansion lower than 0.4%). even if further investigations are required to conclude on a common mechanical behaviour for all sulfate attacks, these experimental

results might be used to evaluate the stress effect on expansion due to external sulfate attack (ESA) and to validate the modelling of ESA-expansion for reinforced structures. Assuming that ASR and DEF have similar mechanical effects on concrete, Charlwood's empirical law has been applied here. Although it has been compared with few experimental points, restrained DEF expansion assessments using this law are conclusive. Another semi-empirical model, proposed by Karthik et al., has also been used. Once again, calculated results are very close to experimental ones. This model presents the advantages of being more convenient from engineering side, thanks to the few physical input parameters needed, and applicable to reinforced concrete provided that the external stress state is known.

Concerning the findings, two major points could be deduced from the different cases of restraint applied in this study in order to obtain relevant modelling of the behaviour of DEF affected concrete under stresses. The first main point provided is the link between anisotropic loading and anisotropic swelling. The second issue is the reduction of the volumetric strain induced by DEF when expansions are restrained. Moreover, expansion induced by sulfate attack in one direction appears to be independent of stress in other directions. It can be evaluated without consideration of the mechanical loading in perpendicular directions. These conclusions are important issues for the development of structural modelling. It has been also highlighted that empirical models based on restrained expansion cannot be used for reassessment and prediction of loaded structures. In this context, poromechanical modelling of DEF affected concrete appears to be relevant. Indeed, a poromechanical law can be used to link poral pressure, external and internal stresses, delayed strains (shrinkage, creep…) and concrete damage. Consequently, interactions between these phenomena can be taken into account. Such modelling of structures damage by internal swelling reaction (ASR or DEF) have been proposed by Morenon et al. [44,48].

Acknowledgements

This work was carried out at LMDC (Laboratoire Matériaux et Durabilité des Constructions) Toulouse in collaboration with and with support from "VINCI Construction Grands Projets" Scientific Department, "VINCI Construction France", "Cofiroute" and "Sixense Concrete".

References

[1] P.K. Mehta, Mechanism of expansion associated with ettringite formation, Cem. Concr. Res. 3 (1973) 1–6. doi:10.1016/0008-8846(73)90056-2.

[2] P.K. Mehta, Mechanism of sulfate attack on portland cement concrete — Another look, Cem. Concr. Res. 13 (1983) 401–406. doi:10.1016/0008-8846(83)90040-6.

[3] C. Ouyang, A. Nanni, W.F. Chang, Internal and external sources of sulfate ions in portland cement mortar: two types of chemical attack, Cem. Concr. Res. 18 (1988) 699–709. doi:10.1016/0008-8846(88)90092-0.

[4] M.C. Lewis, K.L. Scrivener, S. Kelham, Heat Curing and Delayed Ettringite Formation, MRS Online Proc. Libr. Arch. 370 (1994). doi:10.1557/PROC-370-67.

[5] S. Diamond, Delayed ettringite formation — Processes and problems, Cem. Concr. Compos. 18 (1996) 205–215. doi:10.1016/0958-9465(96)00017-0.

[6] M. Collepardi, A state-of-the-art review on delayed ettringite attack on concrete, Cem. Concr. Compos. 25 (2003) 401–407. doi:10.1016/S0958-9465(02)00080-X.

[7] Z. Zhang, J. Olek, S. Diamond, Studies on delayed ettringite formation in early-age, heat-cured mortars: I. Expansion measurements, changes in dynamic modulus of elasticity, and weight gains, Cem. Concr. Res. 32 (2002) 1729–1736. doi:10.1016/S0008-8846(02)00862-1.

[8] H. Bouzabata, S. Multon, A. Sellier, H. Houari, Effects of restraint on expansion due to delayed ettringite formation, Cem. Concr. Res. 42 (2012) 1024–1031. doi:10.1016/j.cemconres.2012.04.001.

[9] A. Pavoine, X. Brunetaud, L. Divet, The impact of cement parameters on Delayed Ettringite Formation, Cem. Concr. Compos. 34 (2012) 521–528. doi:10.1016/j.cemconcomp.2011.11.012.

[10] M.M. Karthik, J.B. Mander, S. Hurlebaus, Deterioration data of a large-scale reinforced concrete specimen with severe ASR/DEF deterioration, Constr. Build. Mater. 124 (2016) 20–30. doi:10.1016/j.conbuildmat.2016.07.072.

[11] X. Brunetaud, Étude de l'influence de différents paramètres et de leurs interactions sur la cinétique de l'amplitude de la réaction sulfatique interne au béton, phdthesis, Châtenay-Malabry, École centrale Paris, 2005. http://www.theses.fr/2005ECAP1025 (accessed March 15, 2016).

[12] S. Bae, O. Bayrak, J.O. Jirsa, R.E. Klingner, Anchor bolt behavior in ASR/DEF-damaged drilled shafts, University of Texas at Austin, Austin, Texas, 2007.

[13] B. Burgher, A. Thibonnier, K.J. Folliard, T. Ley, M. Thomas, Investigation of the internal stresses causes by delayed ettringite formation in concrete, Center for Transportation Research, the University of Texas at Austin, 2004. http://www4.cc.utexas.edu/research/ctr/pdf_reports/0_4713_P2.pdf (accessed March 16, 2016).

[14] D.J. Deschenes, O. Bayrak, K.J. Folliard, ASR/DEF-damaged bent caps : shear tests and field implications, Ferguson Structural Engineering Laboratory - University of Texas at Austin, Austin, Texas, 2009.

[15] M. Thomas, K. Folliard, T. Drimalas, T. Ramlochan, Diagnosing delayed ettringite formation in concrete structures, Cem. Concr. Res. 38 (2008) 841–847. doi:10.1016/j.cemconres.2008.01.003.

[16] B. Godart, L. Divet, Lessons learned from structures damaged by delayed ettringite formation and the French prevention strategy, in: 2013: p. 12p. https://hal.archives-ouvertes.fr/hal-00945667/document (accessed March 16, 2016).

[17] B. Godart, Pathology, Assessment and Treatment of Structures Affected by Delayed Ettringite Formation, Struct. Eng. Int. 27 (2017) 362–369. doi:10.2749/101686617X14881932436771.

[18] P.W. Brown, J.V. Bothe, The stability of ettringite, Adv. Cem. Res. 5 (1993) 47–63. doi:10.1680/adcr.1993.5.18.47.

[19] Y. Fu, P. Xie, P. Gu, J.J. Beaudoin, Effect of temperature on sulphate adsorption/desorption by tricalcium silicate hydrates, Cem. Concr. Res. 24 (1994) 1428–1432. doi:10.1016/0008-8846(94)90156-2.

[20] H.F.W. Taylor, C. Famy, K.L. Scrivener, Delayed ettringite formation, Cem. Concr. Res. 31 (2001) 683–693. doi:10.1016/S0008-8846(01)00466-5.

[21] K. Scrivener, J.P. Skalny, Conclusions of the International RILEM TC 186-ISA Workshop on Internal Sulfate Attack and Delayed Ettringite Formation (4–6 September 2002, Villars, Switzerland), Mater. Struct. 38 (n.d.) 659–663. doi:10.1007/BF02481597.

[22] Y. Shimada, J.F. Young, Thermal stability of ettringite in alkaline solutions at 80 °C, Cem. Concr. Res. 34 (2004) 2261–2268. doi:10.1016/j.cemconres.2004.04.008.

[23] R. Barbarulo, H. Peycelon, S. Leclercq, Chemical equilibria between C–S–H and ettringite, at 20 and 85 °C, Cem. Concr. Res. 37 (2007) 1176–1181. doi:10.1016/j.cemconres.2007.04.013.

[24] X. Brunetaud, R. Linder, L. Divet, D. Duragrin, D. Damidot, Effect of curing conditions and concrete mix design on the expansion generated by delayed ettringite formation, Mater. Struct. 40 (2006) 567–578. doi:10.1617/s11527-006-9163-3.

[25] R.P. Martin, C. BAZIN, J. BILLO, M. ESTIVIN, J.C. Renaud, F. Toutlemonde, Experimental evidence for understanding DEF Sensitivity to early-age thermal history, in: RILEM-JCI Int. Workshop Crack Control Mass Concr. Relat. Issues Early-Age Concr. Struct., France, 2012: p. 10p. https://hal.archives-ouvertes.fr/hal-00851462 (accessed March 15, 2016).

[26] W. Müllauer, R.E. Beddoe, D. Heinz, Sulfate attack expansion mechanisms, Cem. Concr. Res. 52 (2013) 208–215. doi:10.1016/j.cemconres.2013.07.005.

[27] R.-P. Martin, Analyse sur structures modèles des effets mécaniques de la réaction sulfatique interne du béton, phdthesis, Université Paris-Est, 2010. https://pastel.archives-ouvertes.fr/tel-00558200/document (accessed March 16, 2016).

[28] C. Famy, K.L. Scrivener, A. Atkinson, A.R. Brough, Influence of the storage conditions on the dimensional changes of heat-cured mortars, Cem. Concr. Res. 31 (2001) 795–803. doi:10.1016/S0008-8846(01)00480-X.

[29] G. Escadeillas, J.-E. Aubert, M. Segerer, W. Prince, Some factors affecting delayed ettringite formation in heat-cured mortars, Cem. Concr. Res. 37 (2007) 1445–1452. doi:10.1016/j.cemconres.2007.07.004.

[30] N. Leklou, Contribution à la connaissance de la réaction sulfatique interne, phdthesis, L ’UNIVERSITE PAUL-SABATIER TOULOUSE III, 2008. https://hal.archives-ouvertes.fr/tel-01086605/document (accessed March 16, 2016).

[31] H. Bouzabata, S. Multon, A. Sellier, H. Houari, Swellings due to alkali-silica reaction and delayed ettringite formation: Characterisation of expansion isotropy and effect of moisture conditions, Cem. Concr. Compos. 34 (2012) 349–356. doi:10.1016/j.cemconcomp.2011.10.006.

[32] R.-P. Martin, O. Omikrine Metalssi, F. Toutlemonde, Importance of considering the coupling between transfer properties, alkali leaching and expansion in the modelling of concrete beams affected by internal swelling reactions, Constr. Build. Mater. 49 (2013) 23–30. doi:10.1016/j.conbuildmat.2013.08.008.

[33] AFNOR, NF P18-594 - Granulats - Méthodes d’essai de réactivité aux alcalis, 2015.

[34] A. Pavoine, Evaluation du potentiel de réactivité des bétons vis-àvis de la formation différée de l’ettringite, Université Pierre et Marie Curie-Paris VI, 2003.

http://www.efbeton.com/_template/_medias/publications/pdfs/these-pavoine.pdf (accessed June 29, 2016).

[35] H. Cagnon, T. Vidal, A. Sellier, X. Bourbon, G. Camps, Drying creep in cyclic humidity conditions, Cem. Concr. Res. 76 (2015) 91–97. doi:10.1016/j.cemconres.2015.05.015.

[36] W. Ladaoui, T. Vidal, A. Sellier, X. Bourbon, Effect of a temperature change from 20 to 50°C on the basic creep of HPC and HPFRC, Mater. Struct. (2011) 1629–1639.

[37] W. Ladaoui, T. Vidal, A. Sellier, X. Bourbon, Analysis of interactions between damage and basic creep of HPC and HPFRC heated between 20 and 80°C, Mater. Struct. (2013) 13–23.

[38] AFNOR, NF EN 1992-1 - Calcul des structures en béton (Eurocode 2), 2005.

[39] C.W. Correns, Growth and dissolution of crystals under linear pressure, Discuss. Faraday Soc. 5 (1949) 267–271.

[40] G.W. Scherer, Stress from crystallization of salt, Cem. Concr. Res. 34 (2004) 1613–1624. doi:10.1016/j.cemconres.2003.12.034.

[41] L. Divet, Les réactions sulfatiques internes au béton : contribution à l'étude des mécanismes de la formation différée de l'ettringite, IFFSTAR, 2001.

[42] P.K. Mehta, Scanning electron micrographic studies of ettringite formation, Cem. Concr. Res. 6 (1976) 169–182. doi:10.1016/0008-8846(76)90115-0.

[43] O.R. Batic, C.A. Milanesi, P.J. Maiza, S.A. Marfil, Secondary ettringite formation in concrete subjected to different curing conditions, Cem. Concr. Res. 30 (2000) 1407–1412. doi:10.1016/S0008-8846(00)00343-4.

[44] P. Morenon, S. Multon, A. Sellier, E. Grimal, F. Hamon, E. Bourdarot, Impact of stresses and restraints on ASR expansion, Constr. Build. Mater. 140 (2017) 58–74. doi:10.1016/j.conbuildmat.2017.02.067.

[45] R.G. Charlwood, AAR in dams and hydroelectric plants, (2009).

[46] M.M. Karthik, J.B. Mander, S. Hurlebaus, ASR/DEF related expansion in structural concrete: Model development and validation, Constr. Build. Mater. 128 (2016) 238–247. doi:10.1016/j.conbuildmat.2016.10.084.

[47] M.M. Karthik, J.B. Mander, S. Hurlebaus, Modeling ASR/DEF expansion strains in large reinforced concrete specimens, J. Struct. Eng. 144 (2018) 04018085. doi:10.1061/(ASCE)ST.1943-541X.0002030.

[48] P. Morenon, Modélisation des réactions de gonflement interne des bétons avec prise en compte des couplages poro-mécaniques et chimiques, phd, Université de Toulouse, Université Toulouse III - Paul Sabatier, 2017. http://thesesups.ups-tlse.fr/3603/ (accessed April 16, 2018).